HTML ABSTRACT * LINKS

JOURNAL OF APPLIED PHYSICS VOLUME 96, NUMBER 11 1 DECEMBER 2004

## APPLIED PHYSICS REVIEW—FOCUSED REVIEW

# Ion-beam-induced amorphization and recrystallization in silicon

Lourdes Pelaz, Luis A. Marqués, and Juan Barbolla
*Departamento de Electrónica, Universidad de Valladolid, E.T.S.I. de Telecomunicación, 47011 Valladolid, Spain*

(Received 11 May 2004; accepted 5 August 2004)

Ion-beam-induced amorphization in Si has attracted significant interest since the beginning of the use of ion implantation for the fabrication of Si devices. A number of theoretical calculations and experiments were designed to provide a better understanding of the mechanisms behind the crystal-to-amorphous transition in Si. Nowadays, a renewed interest in the modeling of amorphization mechanisms at atomic level has arisen due to the use of preamorphizing implants and high dopant implantation doses for the fabrication of nanometric-scale Si devices. In this paper we will describe the most significant experimental observations related to the ion-beam-induced amorphization in Si and the models that have been developed to describe the process. Amorphous Si formation by ion implantation is the result of a critical balance between the damage generation and its annihilation. Implantation cascades generate different damage configurations going from isolated point defects and point defect clusters in essentially crystalline Si to amorphous pockets and continuous amorphous layers. The superlinear trend in the damage accumulation with dose and the existence of an ion mass depending critical temperature above which it is not possible to amorphize are some of the intriguing features of the ion-beam-induced amorphization in Si. Phenomenological models were developed in an attempt to explain the experimental observations, as well as other more recent atomistic models based on particular defects. Under traditional models, amorphization is envisaged to occur through the overlap of isolated damaged regions created by individual ions (heterogeneous amorphization) or via the buildup of simple defects (homogeneous amorphization). The development of atomistic amorphization models requires the identification of the lattice defects involved in the amorphization process and the characterization of their annealing behavior. Recently, the amorphization model based on the accumulation and interaction of bond defects or IV pairs has been shown to quantitatively reproduce the experimental observations. Current understanding of amorphous Si formation and its recrystallization, predictive capabilities of amorphization models, and residual damage after regrowth are analyzed. © *2004 American Institute of Physics*. [DOI: 10.1063/1.1808484]

### TABLE OF CONTENTS

I. INTRODUCTION . . . 5948
II. PROPERTIES OF AMORPHOUS Si . . . 5949
A. Structural and thermodynamic properties . . . 5949
B. Features of the amorphous phase . . . 5951
1. Transmission electron microscopy (TEM). 5951
2. Double crystal diffractometry . . . 5952
3. Rutherford backscattering (RBS) . . . 5952
4. Raman spectroscopy . . . 5953
5. Electron spin resonance (ESR) . . . 5953
6. Infrared (IR) spectroscopy . . . 5953
III. ION-BEAM-INDUCED DAMAGE AND DYNAMIC ANNEALING . . . 5953
A. Damage generation: displacement cascades . . 5953
B. Damage annealing . . . 5954
IV. KINETICS OF DAMAGE ACCUMULATION . . . 5955
A. Dose: superlinear damage accumulation . . . 5956
B. Ion mass . . . 5956
C. Energy . . . 5957
D. Implant temperature: the critical regime . . . 5957
E. Dose rate . . . 5959
V. MODELS FOR AMORPHIZATION . . . 5959
A. Critical energy/defect density model . . . 5960
B. Overlap damage model . . . 5961
C. Nucleation limited model . . . 5962
D. Defect-based models . . . 5962
1. Vacancies and vacancy complexes . . . 5963
2. Self-interstitial clusters . . . 5963
3. Divacancies and di-interstitial pairs . . . 5963
4. IV pair or bond defect . . . 5964
5. Dangling bonds . . . 5965
6. Kinks on terraces . . . 5965
VI. ATOMISTIC CHARACTERIZATION OF THE AMORPHIZATION PROCESS . . . 5965
A. Molecular dynamics simulations . . . 5966
1. IV pair structure and stability . . . 5966
2. Amorphization by IV pair accumulation . . 5966
3. Influence of the damage morphology . . . 5968
B. Kinetic Monte Carlo simulations . . . 5969
1. Description of the model . . . 5969

0021-8979/2004/96(11)/5947/30/$22.00  © 2004 American Institute of Physics

Downloaded 28 Oct 2008 to 192.84.153.250. Redistribution subject to AIP license or copyright; see http://jap.aip.org/jap/copyright.jsp

2. Morphology and annealing behavior of amorphous regions. . . . . . . . . . . . . . . . . . . . 5969
3. Kinetics of damage accumulation. . . . . . . . 5970
4. Residual damage after regrowth. . . . . . . . . 5971
VII. CONCLUSIONS. . . . . . . . . . . . . . . . . . . . . . . . . . . 5973

## I. INTRODUCTION

Radiation effects in crystalline silicon (*c*-Si) associated to ion implantation, including the crystalline-to-amorphous (*c*-*a*) phase transformation, have been an active area of research because of the use of this technology in the semiconductor industry. Irradiation-induced solid-state amorphization was first noted in experiments on intermetallic compounds,[1] and has been ascribed to either chemical disordering[2] or volumetric expansion of the crystal.[3] In Si, amorphization occurs under ion irradiation when the free energy of the damaged crystalline phase is higher than that of the amorphous phase. In addition to ion implantation, *c*-Si undergoes amorphization far below the melting temperature by various ways such as deposition techniques (vacuum, sputtering, chemical vapor deposition),[4] surface scratch,[5] and indentation.[6] In contrast to metallic alloys and compounds, the ordinary rapid cooling of the melt does not lead to amorphous silicon (*a*-Si) except for laser melting followed by quenching.[7]

Ion implantation is the most commonly used technique to introduce dopants in Si.[8] The passage of an energetic ion through the Si lattice initiates a sequence of displacement events that leads to defect production and, at sufficiently high doses, to the *c*-*a* transformation of the irradiated area. Postimplant thermal processing is required to anneal out the damage and to electrically activate the introduced dopants. The formation of the amorphous phase is beneficial because it limits ion channeling (which can distort the implanted dopant profile) and also it is easily annealed. Annealing, which occurs by solid phase epitaxial growth (SPEG),[9] results in a low defect density in the recrystallized volume and incorporates the dopants into electrically active positions.[10–12] This behavior differs from the regrowth of highly damaged but not continuous amorphous layers. In these cases, annealing temperatures of 800–1000 °C are required to remove extended defects in the implanted region and place all of the dopants into substitutional positions.

The diffusion of dopants in implanted Si is affected by the presence of implantation damage. As an example, the diffusivity of B in implanted single crystal Si is anomalously high compared to equilibrium values. This transient enhanced diffusion (TED) of B and other interstitial diffusers results as a consequence of the supersaturation of Si self-interstitials generated during ion implantation (see Ref. 13 and references therein). This phenomenon has important consequences for Si processing, since it causes a significant spreading of the as-implanted dopant profiles during the subsequent annealing steps required for dopant activation. Ion-induced defects also cause the formation of dopant-defect clusters that prevent complete electrical activation for dopant concentrations well below the equilibrium solid solubility.[14] Because of the technological relevance, a number of experimental works in the field have allowed the characterization of simple and extended defects resulting from implantation and annealing.[15–20] Theoretical models have been developed to describe the observed defect evolution[21–23] and its correlation with dopant diffusion and clustering.[24–31]

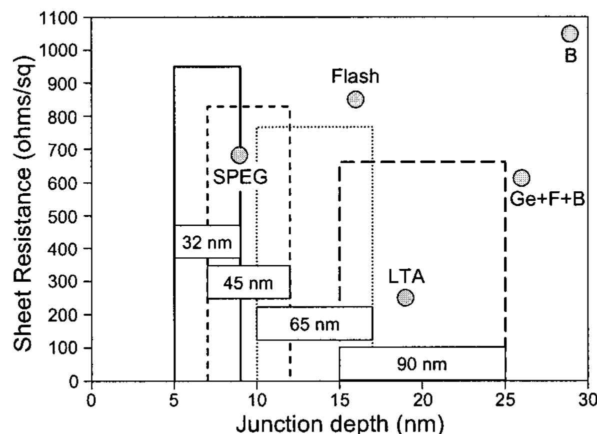


FIG. 1. Sheet resistance vs electrical junction depth in a comparison of promising junction approaches for 90 nm C-MOS and below (after Ref. 32).

As the lateral dimensions of the MOS transistor channel are scaled down, the source/drain extension junction depth must be proportionately reduced in order to avoid short-channel effects. At the same time, the sheet resistance of the source/drain extension regions must be decreased so that they do not add a significant resistance to the channel resistance. Conventionally there is a compromise involved in maximizing dopant activation while minimizing dopant diffusion. High annealing temperatures are required to activate the dopants, but significant diffusion occurs during this process. Different techniques have been proposed to improve simultaneously the sheet resistance and the junction depth,[32] such as the coimplantation of B with Ge and F and the use of aggressive annealing processes, such as flash or laser thermal annealing (LTA).[33] SPEG of preamorphized samples has been shown to improve B activation with minimal diffusion.[34,35] Thus, this technique appears to be a promising method to achieve the sheet resistance and junction depth specifications for the 45 nm node, as shown in Fig. 1.

The development of predictive computer models that allow the optimization of technological processes without the need of expensive experimental tests has been pointed out in the successive International Technology Roadmap for Semiconductors editions.[36] In particular, the importance of the understanding and modeling of the *c*-*a* transition has been recognized. In the 2001 edition the following is stated: "More detailed understanding of implant damage, amorphization and subsequent recrystallization is important, as these phenomena can critically affect dopant profiles [...] Extensive research and model development needs to be started immediately to develop improved models for damage creation and annealing, and for temperature-dependent implantation."

Traditionally, amorphization was modeled in a very simplistic way. It was assumed that the lattice turned amorphous if a critical point defect concentration was exceeded.[37] Recrystallization occurred instantaneously, resulting in a free-of-defects crystalline zone. Only defects beyond the

Downloaded 28 Oct 2008 to 192.84.153.250. Redistribution subject to AIP license or copyright; see http://jap.aip.org/jap/copyright.jsp

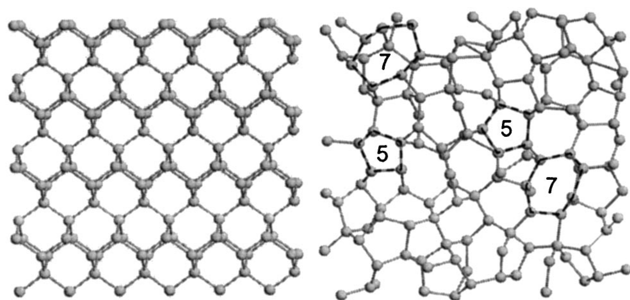


FIG. 2. On the left we show a thin slab (5.43 Å thick) of *c*-Si. Each atom is located in the center of a tetrahedron and bounded with the four atoms of their vertices. Atoms form the six-membered rings typical of the diamond structure. On the right we represent a slab of *a*-Si of the same thickness. Even tough mean coordination is still four, long range order is lost. Five- and seven-membered atom rings are clearly visible.

amorphous-crystalline $(a/c)$ interface remained. One of the main limitations of this simplistic model is the uncertainty in the critical point defect concentration value. Different authors have reported values ranging between $10^{21}$ and $10^{23}$ $cm^{-3}$ depending on the implant parameters (see Ref. 38 and references therein). This uncertainty leads to variations of a few nanometers in the predicted depth of the $a/c$ interface and to changes up to 50% in the residual damage concentration beyond it.[38] The exact amount of the residual damage is of great relevance for technological purposes as it significantly affects dopant diffusion and activation. Therefore, it is essential to develop ion induced amorphization models, compatible with process simulators, which are able to capture the features of the *c*-*a* transition and its dependence on implant parameters.

On the basis of such technological motivations, a great effort has been made to quantitatively understand the kinetics of the ion-beam-induced *c*-*a* transition. A number of models have been developed to describe the experimental observations associated to this phase transformation. How the damage accumulates before the *c*-*a* transition, what are the defects involved in the process, how the different damage structures heal, and how the crystalline structure recovers are some of the questions to be answered.

In this paper we will review the experimental results and theoretical analysis concerning the damage generation and its dynamic anneal, as well as the kinetics of the damage accumulation as a function of the implantation parameters. A number of phenomenological models proposed in the past to explain the experimental results will be commented as well as structure models that try to identify defects responsible for the phase transition. We will focus our attention on an atomistic quantitative model that encompasses previous models and provides a comprehensive understanding of experimental results. The present paper is organized as follows: in Sec. II we will briefly review the properties of *a*-Si and the features used in experimental techniques to quantify different levels of damage and distinguish the crystalline and amorphous phases. We will then present in Sec. III theoretical and experimental observations on damage generation and damage annihilation whose balance will determine the rate of damage accumulation. In Sec. IV the interplaying role between implant parameters (dose, dose rate, ion mass and energy, and substrate temperature) to determine the onset of amorphization will be analyzed. Section V is devoted to the description of existing models for ion-beam-induced amorphization. We will give special emphasis to the interpretation of experimental results within the models. In Sec. VI we will describe an atomistic model for Si amorphization and recrystallization that we have developed, which is able to reproduce all the experimental observations. Finally, we will draw some conclusions in Sec. VII.

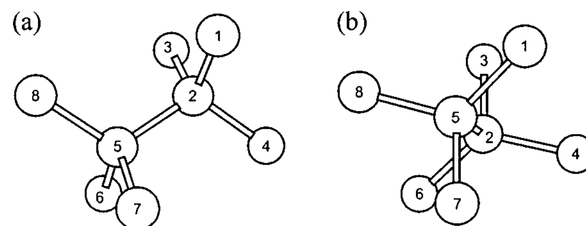


FIG. 3. Local rearrangement of bonds used to generate the WWW model of *a*-Si: (a) configuration of bonds in the perfect diamond lattice and (b) relaxed configuration of atoms after switching the bonds (from Ref. 46).

## II. PROPERTIES OF AMORPHOUS Si

One of the most prominent differences between *a*-Si and *c*-Si is that many properties which are well defined in *c*-Si are found to be variable in *a*-Si and to depend on the thermal history and/or preparation conditions.[39] As an example, *a* -Si prepared by physical vapor deposition (by either vacuum evaporation or sputtering) at high deposition rates on cold substrates shows the formation of nanometer-sized voids.[40] This morphology is often accompanied by a density deficit relative to *c*-Si of more than 10%.[40–42] Measurements of atomic density[43] and dangling bond density[44] indicate that intrinsic atomic density of *a*-Si prepared by ion implantation is only 1.76% less than that of *c*-Si.

### A. Structural and thermodynamic properties

*c*-Si has a diamond cubic lattice with a density of $5 \times 10^{22}$ atom/$cm^3$. Each atom is covalently bonded and fourfold coordinated. The four first nearest neighbors are sitting at the vertices of a tetrahedron. The typical angle subtended between two adjacent bonds is 109.47°. The bond length is of 2.35 Å at 300 K. This arrangement of atoms produces the six-membered rings characteristic of *c*-Si. *a*-Si preserves the fourfold coordination of the atoms, but long-range order is suppressed by distortions of the ideal tetrahedral bond angle. *a*-Si incorporates five- and seven-membered rings mixed with the six-membered rings of the perfect crystal. A comparison of both atomic structures is shown in Fig. 2.

*a*-Si is described ideally as a continuous random network of Si atoms.[45] Wooten, Winer, and Wearie (WWW) developed a computational model to generate semiconductor amorphous structures.[46] It consists of the introduction of local rearrangements of bonds in the diamond lattice (see Fig. 3) weighted by a Maxwell-Boltzmann factor. The WWW model gives an overall good description of the *a*-Si structure; however it predicts an amorphous phase 3%–4% denser than the crystal,[47] contrary to experiments. Besides, the model describes a "perfect" continuous random network, with all

Downloaded 28 Oct 2008 to 192.84.153.250. Redistribution subject to AIP license or copyright; see http://jap.aip.org/jap/copyright.jsp

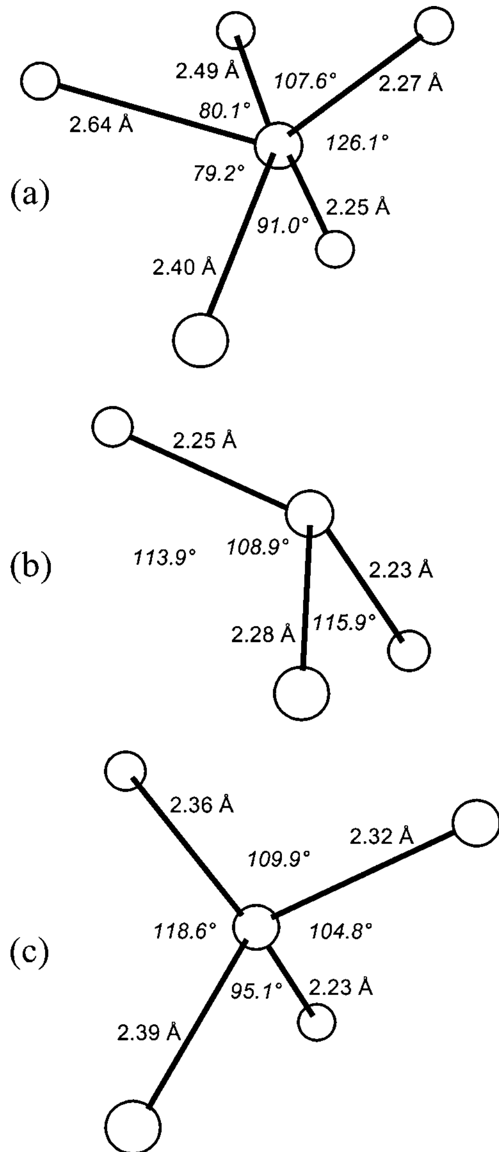


FIG. 4. Atomic structures of (a) the floating bond, (b) the dangling bond, and (c) the highly distorted fourfold coordinated atom. These structures have been obtained using first-principle techniques (from Ref. 50).

the atoms fourfold coordinated, while several experiments have shown that a high concentration of defects is indeed present in the as-implanted material.[39,48–50] Dangling bonds,[51] floating bonds,[52] strained Si-Si bonds,[49] and vacancy-type defects[53] have been suggested as possible defects of the amorphous network. The atomic structures of some of them are shown in Fig. 4.

The presence of large defect concentrations in the structure implies a large average bond angle distortion, with a larger associated free energy. Low temperature processes ($T < 500$ °C) produce modifications in the atomic structure of as-implanted *a*-Si.[40] The vibrational[39,54–56] and optical[57,58] properties, electron-spin density,[49,59,51] and enthalpy[39,60,61] also change. Annealing-induced relaxation effects have been also shown in metal diffusion techniques.[62] The existence of structural relaxation phenomena below room temperature has been observed by *in situ* techniques of strain[63] and conductivity.[49]

Differential scanning calorimetry techniques[39,60,61] show that the as-implanted *a*-Si releases an enthalpy of ~5 kJ/mol during low-temperature annealing toward a relaxed configuration.[60,61] The facts that the release at a particular temperature is small and that the homogeneous release is quite even over a large temperature range suggest the existence of a wide spectrum of activation enthalpies (associated to different defect structures) governing the process. *In situ* conductivity measurements of ion implanted *a*-Si at 77 and 300 K demonstrate the presence of defects with a continuous spectrum of activation energies between 0.3 and 2.7 eV.[49]

The structural relaxation upon thermal annealing has been interpreted in terms of defect annihilation and concomitant bond rearrangement, with a reduction of bond angle distortion. Studies on the annealing kinetics at low temperature show that the annealing rate of defects scales with the square of the defect density, demonstrating that a bimolecular kinetics is operative.[39,49] The concentration of these defects can be reduced by a factor of 5 upon annealing at 800 K with respect to the as-implanted material. With a reimplantation and annealing, samples can be cycled between the as-implanted and the relaxed amorphous states. The dose required to produce the transformation of relaxed *a*-Si to unrelaxed *a*-Si is approximately one order of magnitude less than that required for the amorphization of *c*-Si.[48,64] The data suggest that stable defects are introduced in *a*-Si as a result of nuclear collisions thus causing the derelaxation of the network. Conversely, it would appear that relaxation of the network involves annihilation of these defects.

Both relaxed and unrelaxed *a*-Si show identical densities within experimental error (<0.1% density difference).[43] Since there is no measurable density difference between as-implanted and annealed samples, this implies that the relaxation occurs without significant volume changes. Curvature measurements of Si wafers before, during, and after ion implantation have shown that during structural relaxation *a*-Si does in fact expand even further (by 0.15% to a 1.9% deficit) whereafter it densifies (by 0.1%).[63] It should be emphasized that the relaxed or unrelaxed states of *a*-Si do not necessarily represent different phases of *a*-Si but rather differences in the densities of defect complexes.

Heating at temperatures above 500 °C induces a phase transition from the metastable amorphous phase into the thermodynamically stable crystalline phase.[65–67] The measured enthalpy of crystallization by different techniques is $\Delta H_{ac} \sim 12$ kJ/mol.[60,61,68,69] *a*-Si layers onto single-crystal substrates recrystallize epitaxially[66] by means of a planar motion of the $a/c$ interface.[70] The thermal recrystallization rate of the planar $a/c$ interface exhibits Arrhenius-type behavior.[61,67,70–73] For an *a*-Si layer on top of (100) oriented *c*-Si Olson gave values of the interface velocity, following the expression

$$v_C(\text{cm/s}) = 3.08 \times 10^8 \exp(-2.68 \text{ eV}/k_B T) \tag{1}$$

over a regrowth rate range of more than ten orders of magnitude in the temperature range 500–1400 K.[67] The recrystallization velocity has been demonstrated to depend on substrate orientation.[9,67] For instance, the recrystallization on (110) and (111) oriented substrates is, respectively, 2.5 and

Downloaded 28 Oct 2008 to 192.84.153.250. Redistribution subject to AIP license or copyright; see http://jap.aip.org/jap/copyright.jsp

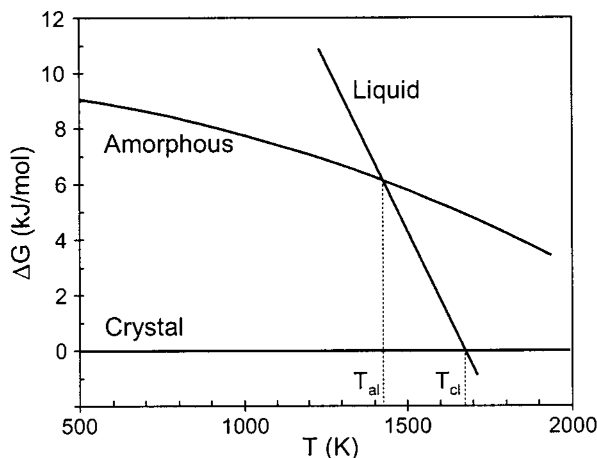


FIG. 5. Phase diagram for Si, where Gibbs free-energy differences for the crystal, liquid, and amorphous phases are represented as a function of temperature. From the line intersection points it is possible to extract the melting temperatures $T_{al}$ and $T_{cl}$ (after Ref. 73).

25 times smaller than on (100) substrates. Another interesting result of the kinetics of SPEG is the strong dependence on the impurity content. Some dopants, such as P, B, As, enhance the growth rate.[67,70,74] The simultaneous presence of *n*-type and *p*-type dopants produces a compensating effect in the growth rate and a suppression of its enhancement.[67,75,76] Other impurities, such as C, O, F, or noble gases, retard the regrowth kinetics and can even halt it.[67,77,78]

In the absence of a preexisting planar $a/c$ interface, the phase transformation starts with the spontaneous formation of microcrystallites in the amorphous matrix.[79,80] Initially, these microcrystals are very small and unstable because of the large surface-to-volume ratio and therefore tend to shrink. However, a few of them will become large enough, above the so-called *critical size*, for their growth to continue. The formation process of crystalline grains of size larger than the critical size is known as *nucleation*. After an incubation period a steady state is reached where the nucleation and grain growth rates become time and grain size independent. The nucleation process in Si has been investigated in a limited temperature range, between 500 and 700 °C.[81–83] In this regime the nucleation and growth rates show Arrhenius behavior, with activation energies of around 5 and 3 eV, respectively.[83] For higher temperatures the behavior will deviate from the Arrhenius type since the free energy difference between the amorphous and crystalline phases decreases.[60]

From the value of $\Delta H_{ac}$ and Gibbs free-energy calculations (see Fig. 5), the melting temperature of *a*-Si has been determined to be $T_{al}=1420$ K, which is a factor 0.84 below the crystal melting temperature, $T_{cl}=1685$ K.[73,84,85] The melting points of annealed and unannealed samples show no difference within the experimental uncertainty. This indicates that the relaxation of the amorphous phase must proceed rapidly at high temperatures to reach the same state prior to melting. The heat of melting of the amorphous phase (obtained by ion implantation) is $\Delta H_{al} \sim 37$ kJ/mol.[84,86] The amorphous-to-liquid phase transition involves a fundamental change in bonding from the covalent, amorphous phase with fourfold coordination to the metallic liquid with 11- 12-fold coordination, suggesting a first-order phase change. The first-order character of the transformation has been demonstrated by laser annealing experiments[87,88] and electron beam pulse heating.[86] The liquid-to-amorphous transition should be reversible so that supercooling the melt beneath $T_{al}$ would lead to growth of *a*-Si in the melt. This has in fact been observed following fast (<2.5 ns) pulsed laser annealings.[86,89]

To sum up, in Table I we list some of the thermodynamic and kinetic data for Si.

### B. Features of the amorphous phase

A number of experimental techniques have been employed in studies of the nature of the damage, the presence of amorphous material, and the kinetics of amorphization and recrystallization associated with ion implantation. Variations in optical, vibrational, or structural properties from the crystalline features to the amorphous signals have been assigned to damage formation. When a *saturation* response is reached, it is interpreted as the formation of a wholly amorphous layer. Sometimes, complementary techniques are used simultaneously in order to distinguish *a*-Si from perfect or damaged crystal. A brief description of the experimental techniques most commonly used to study Si amorphization is presented in the following, as well as the *a*-Si properties in whose detection they are based.

#### 1. Transmission electron microscopy (TEM)

A transmission electron micrograph of *c*-Si shows a pattern of spots whose intensity and spacing depend on Bragg reflection conditions. In lightly damaged *c*-Si, these spots will exhibit faint streaking. As Si is driven toward the amor-

TABLE I. Thermodynamic and kinetic data for Si (after Refs. 73 and 84).

| Physical property | Measured value |
|---|---|
| Melting temperature of the crystal, $T_{cl}$ (K) | 1685 |
| Heat of melting of the crystal, $\Delta H_{cl}$ (kJ/mol) | 50.5 |
| Kinetic crystallization temperature of the amorphous phase, $T_{ac,k}$ (K) | 960 |
| Heat of crystallization of the amorphous phase, $\Delta H_{ac}$ (kJ/mol) | 11.95 |
| Residual entropy of the amorphous phase, $S_a$ (J/mol K) | 1.66 |
| Specific heat difference between the amorphous and crystalline phases, $\Delta C_{p,ac}$ (J/mol K) | $-0.224+4.8(T/1685)$ |
| Melting temperature of the amorphous phase, $T_{al}$ (K) | 1420 |
| Heat of melting of the amorphous phase, $\Delta H_{al}$ (kJ/mol) | 37.1 |

Downloaded 28 Oct 2008 to 192.84.153.250. Redistribution subject to AIP license or copyright; see http://jap.aip.org/jap/copyright.jsp

phous condition, the spot pattern will disappear and, in truly *a*-Si, it will be replaced by a pattern of three concentric rings, called Debye-Scherrer rings.[90] Amorphous zones show a different contrast and the diffraction pattern in the amorphous phase presents characteristic rings. These features are brought out especially clearly in the work of Ishimaru *et al.*[91] and Yamasaki *et al.*[92]

#### 2. Double crystal diffractometry

An expansion of the lattice in *a*-Si occurs to accommodate the decrease in density compared to *c*-Si. Double crystal diffractometry measures the relative difference between the lattice constants of the implanted layer and the substrate. As the damage increases, the x-ray diffraction peak intensity from the implanted layer decreases rapidly, at the same time that the largest angular separation between the diffraction peaks of the implanted layer and the substrate increases. This technique was used to monitor the strain in implanted layers.[93] The perpendicular strain was found to be positive and increases with dose, meaning that the perpendicular lattice spacing in the implanted layer is larger than that of the substrate and increases with the damage in the layer.

Also, from the x-ray intensity $I(Q)$ scattered coherently by $N$ atoms with atomic scattering factor $f(Q)$ it is possible to determine the material structure factor $S(Q)$:[94]

$$S(Q) = \frac{I(Q)}{Nf^2(Q)}. \tag{2}$$

From the structure factor it is possible to calculate *the radial distribution function*, usually represented by $g(r)$:

$$g(r) = 1 + \frac{1}{2\pi^2 r\rho}\int_0^\infty Q[S(Q)-1]\sin(Qr)dQ, \tag{3}$$

where $\rho$ is the atomic density of the material. This function is a measure of the microscopic correlation among the atoms in such a way that $g(r)d(r)$ gives the probability of finding a particle in the elemental volume comprised between the spheres of radii $r$ and $r+dr$ centered on a given one. The radial distribution function is easily calculated in atomistic simulations, which allows the connection between experiment and theoretical models. From the integration of $g(r)$ it is possible to determine meaningful properties of the material.[95] For example, the mean atomic coordination (mac) can be extracted by

$$\mathrm{mac} = 4\pi\rho\int_0^{r_{\min}} r^2 g(r)dr, \tag{4}$$

where $r_{\min}$ is the distance corresponding to the first minimum in $g(r)$.

In the case of Si, the inspection of $g(r)$ allows us to easily infer the aggregation state of the material.[96] As an example, we show in Fig. 6 the radial distribution functions corresponding to crystal, amorphous, and liquid Si extracted from molecular dynamics (MD) simulations (see Sec. VI A). In the case of *c*-Si, peaks in $g(r)$ are well defined at distances corresponding to the first, second, third, and so on neighbor shells. The width of the peaks is related to thermal vibrations. For *a*-Si, there are clear peaks at the first and second neighbor distances typical of the Si lattice, but although local coordination is still four, long-range order is lost. This effect is increased in the case of liquid Si, where first and second peaks merge, with an increase of the mean atomic coordination which gives an indication of its metallic character.[97]

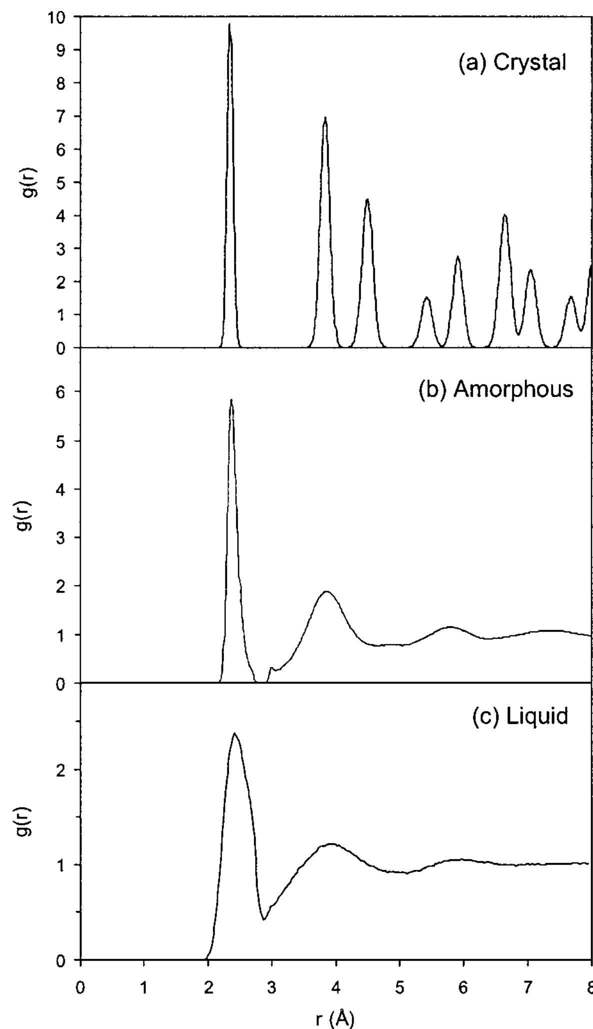


FIG. 6. Radial distribution functions for (a) *c*-Si at room temperature, (b) *a*-Si at room temperature, and (c) liquid Si at the melting point. All of them were obtained from MD simulations.

#### 3. Rutherford backscattering (RBS)

The yield of energetic (typically 1.2 MeV) $He^+$ ions backscattered into a given solid angle is essentially the same for *a*-Si and *c*-Si oriented in a nonchanneling direction with respect to the He beam, but channeling directions can be found in crystalline material for which a large decrease in the backscattering yield is obtained. From a backscattering viewpoint, damaged Si appears to be amorphous when the backscattering yield is independent of the direction of the probing beam and has a magnitude equal to the yield obtained from a single crystal oriented in a nonchanneling direction. Since lattice atoms displaced more than 0.2 Å give a contribution to the backscattering yield, RBS measurements give an increasing scattering yield as the damage increases.[98–100] The damage contributing to a well-resolved peak in RBS consists

Downloaded 28 Oct 2008 to 192.84.153.250. Redistribution subject to AIP license or copyright; see http://jap.aip.org/jap/copyright.jsp

of grossly displaced Si atoms, i.e., individual interstitial atoms, interstitial clusters, and amorphous regions. Other types of damage, such as vacancies (with their associated relaxation of neighboring lattice atoms), dislocations, or lattice strain, only enhance the dechanneling rate and hence increase the scattering yield from all larger depths but they do not normally produce a resolvable damage peak.[101]

#### 4. Raman spectroscopy

In *c*-Si there is a sharp Raman peak centered at 520 $cm^{-1}$ while a broad peak centered at 480 $cm^{-1}$ is characteristic of *a*-Si. The *c*-Si Raman peak at 520 $cm^{-1}$ corresponds to the triply degenerate $K=0$ transverse optical (TO) phonon modes and a weak peak at 305 $cm^{-1}$ is due to two phonon transitions. The broad peak of *a*-Si has contributions from all TO phonon modes.[102] As the damage increases, the *c*-Si Raman peak at 520 $cm^{-1}$ decreases, broads, and shifts toward lower wave numbers and the *a*-Si peak becomes predominant.[102–104] These peak shifts as damage increases can be attributed to uniaxial lattice expansion in the direction normal to the Si surface.[103] It has been shown that there is a linear relationship between bond-angle deviation $\Delta\theta$ from the tetrahedral angle (typically ranging from 7° to 13°) and the peak width of the *a*-Si TO vibrational modes.[105,106] This technique has been used to evaluate the relaxation of as-implanted *a*-Si,[48,106] as well as to characterize different levels of damage.[102–104]

#### 5. Electron spin resonance (ESR)

Dangling bonds (threefold coordinated atoms) and floating bonds (fivefold coordinated atoms) have been suggested as ESR active sites characteristic of the *a*-Si.[52] The ESR signal for *a*-Si consists of a symmetrical Lorentzian isotropic line 7.5 G wide at room temperature, and 4.7 G at 77 and 4.2 K with a *g* value of 2.0055. The magnitude of the spin signal corresponds to a spin density of $2\times10^{20}$ spins/$cm^3$. Normally, it is assumed that the intensity of the ESR line is directly proportional to the amount of *a*-Si present in the implanted layer.[107–109] Undoped *c*-Si shows no such line, though divacancies and other crystalline defects have readily identifiable spin resonance signals.

#### 6. Infrared (IR) spectroscopy

*c*-Si has a sharp optical absorption edge at a wavelength of $1.1\mu$, while *a*-Si has a more gradual optical absorption edge starting at about $1.25\mu$. Disordered Si that is not completely amorphous will also show a divacancy absorption band at a wavelength of $1.8\mu$, though this band disappears when the material is truly amorphous.[110] The presence of damage raises the refractive index near the fundamental absorption edge in Si $[\lambda=(1-2)\mu]$.[64,111–113] Changes in the refractive index have been associated to changes in the relative volume of the amorphous phase within the crystal.[111] Interference fringes observed in IR transmission measurements caused by small difference in the index of refraction between *a*-Si and *c*-Si permit the measurement of the amorphous layer depth.

## III. ION-BEAM-INDUCED DAMAGE AND DYNAMIC ANNEALING

The mechanisms of defect production and dynamic annealing during ion bombardment represent crucial information for the description of a variety of nonequilibrium phenomena occurring under ion irradiation. The strike of an energetic ion into a solid generates a sequence of atomic displacements that leads to free energy changes and, ultimately, to the *c*-*a* transformation of the irradiated sample. In order to be able to understand the physical mechanisms of defect accumulation and phase transformation, it is important to analyze not only the defect production process itself but also the evolution of the generated damage, since heating of the sample may cause some damage healing and even prevent amorphization.

### A. Damage generation: displacement cascades

Ion-solid interactions can induce structural modifications due to the transfer of energy from the impinging ions to the target atoms. A threshold energy of 15–20 eV is required to create a Frenkel pair.[114–116] If the energy transfer is lower only local heating occurs, which is known as the *thermal spike* regime. When ions transfer much higher energy to target Si atoms than needed to create a Frenkel pair, the interaction of displaced atoms with other lattice atoms can lead to further displacements (recoils). Frenkel pair production is therefore a cascade process in which the incident ion is simply the primary damage-producing particle. The total of all such events is commonly referred to as the *collision cascade* of the ion. High defect densities are generally associated with the vicinity of the ion track, especially near the end of range (EOR) where the ion's velocity is sufficiently slow so that nearly every atomic interaction results in a displacement event.[117]

The small size ($\sim10^{-25}$ $cm^3$) and short lifetime ($\sim10^{-11}$ s) of the displacement cascades generated along the path of an energetic beam make their investigation by experimental means very difficult; only indirectly can the primary state of damage be inferred. Theoretical models permit us to estimate the number of atoms displaced by a projectile as it comes to rest and provide an approximate indication of the damage produced by implantation. MD simulation methods[95] and computer simulation codes based on the binary collision approximation (BCA),[118] such as TRIM (Ref. 119) and MARLOWE,[120] as well as analytical descriptions based on linear Boltzmann transport theory,[121] have generally been used for this purpose. Within the BCA approximation, the collisions between recoils in the ion-induced displacement cascade occur only between moving and stationary atoms. The MD technique in turn treats the full dynamics of the collision processes, and consequently it is more precise for low recoil energies (<200 eV), at the expense of being more computationally demanding.

During the thermal spike regime of the cascade, local heating can lead to the melting of significant volumes of material,[122] and thus it can have an important role on amorphization. Brinkman considers that the damage could be formed during cascade quenching as a result of collective

Downloaded 28 Oct 2008 to 192.84.153.250. Redistribution subject to AIP license or copyright; see http://jap.aip.org/jap/copyright.jsp

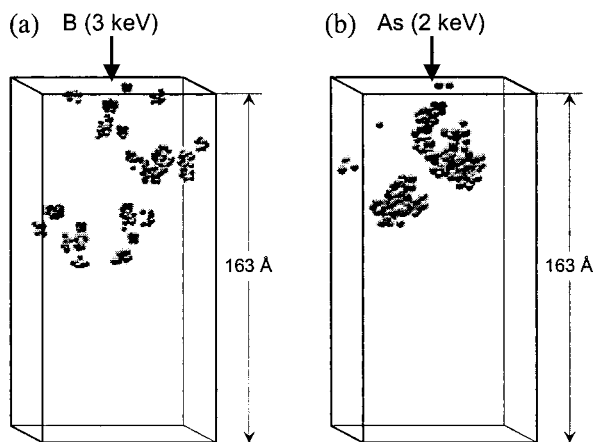


FIG. 7. Morphology of the damage created by the implantation of (a) a 3 keV B ion and (b) a 2 keV As ion, as obtained by MD techniques. The damage energy is the same for both ions (1.3 keV). Atoms displayed have a potential energy 0.2 eV higher than the reference crystal. While B creates mainly isolated Frenkel pairs and small clusters, As produces more extended disordered zones (after Ref. 125).

atomic motion within the cascade volume.[117] In metal systems, the thermal spike does not result in amorphization, and resolidification of the local melt absorbs many of the Frenkel pairs produced during the early collisional stages. Thus, in metals the final number of defects after the thermal spike is reduced relative to the production during the early collisional stages and, therefore, relative to the BCA predictions.[123] On the contrary, in Si, local melting of the cascade core results in amorphous pockets. The solidification of the locally molten cascade zone occurs at a rate between $10^{14}$ and $10^{15}$ K/s, which in Si leads to interface velocities much larger than the critical velocity for amorphization.[124] Detailed MD simulations indicate that amorphous pockets contain many more displaced atoms than just simply those produced directly in high energy binary collisions.[122]

Also from MD simulations, Caturla *et al.* provide quantitative information at the atomic level on the nature of implantation damage in Si under a wide variety of conditions.[125] When implanting B and As ions of the same damage energy into *c*-Si, the resulting morphology of the damage is substantially different, as shown in Fig. 7. In the case of the B cascade a number of isolated Frenkel pairs and small clusters are observed. Since local melting in the cascade does not take place for low mass ions, defect production is essentially governed by the early ballistic phase of the cascade and therefore agrees well with the BCA predictions at low temperatures. Defects can be reduced over time due to bulk recombination and annihilation at surfaces and internal sinks, and the experimental RBS profiles at room temperature can give smaller amount of defects than those predicted by BCA calculations. In As irradiation and other high-mass ions such as In and Sb, the damage is mostly in the form of large defect clusters and amorphous pockets, indicating that for high-mass ions the damage morphology is governed by local melting in the cascade core which upon resolidification results in local amorphous pockets. The energy per atom required to melt the material in the cascade region is much smaller than the threshold energy to form a Frenkel pair. Intracascade amorphization results in large damage volumes per cascade, and therefore in more displaced atoms off lattice sites than predicted by BCA. The presence of discrete amorphous zones produced by very heavy ion (Bi) implantation at room temperature has also been observed in TEM images.[126,127]

Differences in the damage morphology produced by different ions affect its annealing behavior, and thus the damage accumulation. Whether amorphization is the result of homogeneous accumulation of point defects or it happens as a consequence of the heterogeneous overlap of amorphous pockets formed by successive collision cascades has been a subject of intense debate.[107,109,128] These ideas will be reviewed in Sec. IV.

## B. Damage annealing

The annealing behavior of the damaged regions reveals various stages and temperatures for significant defect recovery, indicating that the damage consists of a hierarchy of various defect structures.

Single interstitials and vacancies diffuse at temperatures lower than room temperature,[129] di-interstitials anneal at 150 °C,[130] and divacancies anneal at 100–250 °C.[131] Simple defects can agglomerate and form extended defect clusters of Si interstitials,[16] such as {113} defects[15] or dislocation loops,[132] or clusters of vacancies and cavities,[133] which require annealing temperatures of 800–1000 °C to be removed. The dissolution of these defects involves the emission of point defects that diffuse until they are annihilated at the surface.[15] On their way to the surface point defects may also interact with dopant atoms resulting in enhanced dopant diffusion and dopant clustering (see Refs. 13 and 24, and references therein).

The disorder created by light ions recovers faster and to a much larger extend than that produced by heavier ions.[125] Discrete amorphous regions (nanometer sized) produced by very heavy ions[126,127,134,135] or low-temperature implants[136,137] regrow at temperatures below 400 °C. This temperature is significantly lower than in the case of a planar $a/c$ interface, which regrows with appreciable rate above 550 °C.[65] Low-temperature regrowth of damaged regions has also been observed in the nonplanar $a/c$ interfaces formed by liquid nitrogen temperature implants.[137] However, once the interface becomes sharp, an increase in temperature is required to continue the layer-by-layer SPEG.[138] This enhanced regrowth of discrete amorphous regions or nonplanar $a/c$ interfaces is significantly higher than that expected from the simultaneous growth at each of the many interfaces of isolated or irregular amorphous regions. Nelson proposed that the recrystallization kinetics of the isolated amorphous zones in Si depends on their average diameter due to surface-energy effects.[139] As the diameter decreases the contribution of the surface energy to the total free energy of the amorphous phase will increase, resulting in a larger driving force for crystallization. However, differences in this driving force cannot account for the large variations in the interface-controlled kinetics.

Downloaded 28 Oct 2008 to 192.84.153.250. Redistribution subject to AIP license or copyright; see http://jap.aip.org/jap/copyright.jsp

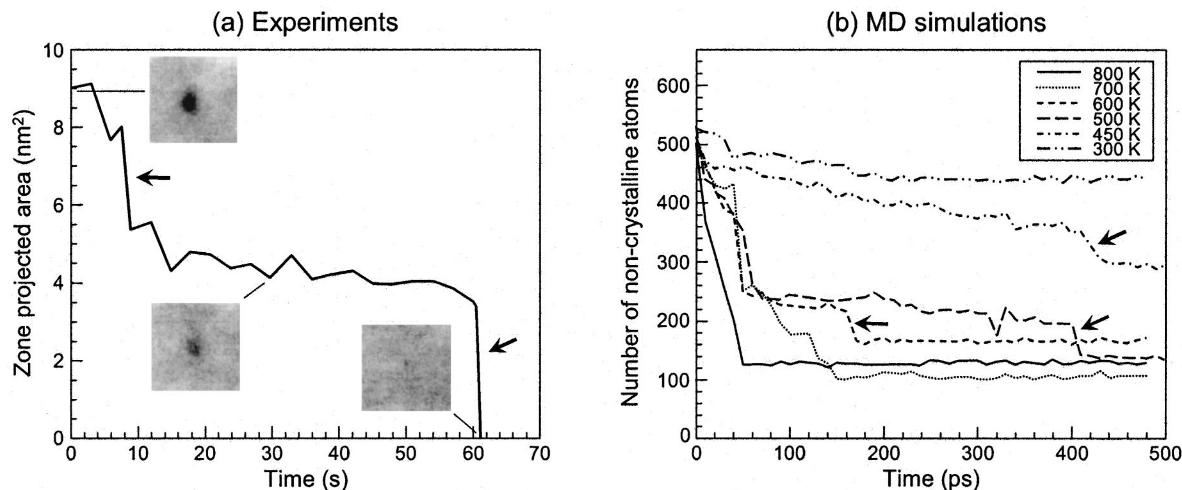


FIG. 8. (a) Experimentally measured recrystallization behavior at 300 °C of a single amorphous zone created by 200 keV Xe ion irradiation (from Ref. 140). (b) Number of atoms in an amorphous pocket generated by a 5 keV As implant as a function of time for several temperatures, as obtained using MD techniques (from Ref. 125). Even though the time scales are different, in both cases crystallization does not happen uniformly but with a steplike behavior (indicated by the arrows).

Theoretical[125,141] and experimental[140] observations indicate that the regrowth of these amorphous regions takes place over a wide range of temperatures between 100 and 400 °C. MD simulations predict that the stability of small amorphous zones increases with their size.[125] However, the experimental annealing of individual amorphous zones shows little or no correlation between their size and recrystallization temperature: zones with similar starting sizes disappeared (crystallized) at temperatures anywhere from 70 °C to more than 400 °C.[140] This suggests that these defect structures are not in a uniquely defined state. The irregularity of the interface of any nanometer-sized zone and the variation in local atomic arrangement at the interface may be responsible for a wide range of energies and temperatures for recrystallization. Another feature observed experimentally[140] and in theoretical calculations[125] is that recrystallization of amorphous pockets shows plateaus and step regions, as shown in Fig. 8, instead of showing a smooth exponential decay governed by a unique activation energy. This suggests that recrystallization involves a triggering event, followed by a rapid rearrangement of atoms, as it has also been observed in the growth of planar $a/c$ interfaces.[76] Another similarity with SPEG is that the reordering of damage clusters is also affected by the presence of dopants.[138]

An interesting observation derived from theoretical calculations is that recrystallization of the amorphous pockets occurs without the intervention of point defects external to them.[125] However, amorphous regions often contain a deficit or an excess of atoms when compared with the perfect crystal. MD simulations show that during annealing these regions collapse into clusters of interstitials or vacancies.[122] Analogously, TEM images show that recrystallization of a buried amorphous layer results in the formation of a shell of defects along the plane where the two advancing $a/c$ interfaces merged.[142–144] When the planar interface extends to the surface, the defects are swept at the same time that the recrystallization takes place, leaving only the defects beyond the $a/c$ interface.[145,146]

## IV. KINETICS OF DAMAGE ACCUMULATION

The observation of the building up of the amorphous material as the implantation proceeds can help understand the mechanisms of damage accumulation that eventually leads to amorphization. Point defect, defect complexes, or locally amorphous regions can accumulate as successive cascades are implanted in the target material until highly damaged *c*-Si becomes unstable and transforms into *a*-Si. In fact, RBS measurements indicate that ion-beam-induced amorphization occurred initially near the most heavily damaged region (near the EOR).[102–104,128] Continued irradiation increases the thickness of the generated amorphous layer. For Si implanted ions into Si at room temperature a planar layer with distinct sharp interfaces on either side separating amorphous from crystalline Si appears. For implantations at liquid nitrogen temperature there is an occurrence of the amorphous islands over the entire range of the ion and the interface does not appear sharp in TEM images.[91,136,137]

Irradiation into a planar amorphous layer[147] or amorphous clusters[135,138,148] may produce additional amorphization or layer by layer recrystallization, depending on the temperature of the substrate and on the dose rate.[56,98,147] The activation energy of ion-beam induced epitaxial crystallization (IBIEC) is found to be varied from 0.18 to 0.40 eV depending on ion mass and temperature.[98,147,149–154]

Amorphization is hampered when Si is irradiated at elevated temperatures. However, defects existing previously to irradiation can act as nucleation sites for amorphization. Free surfaces,[155] grain boundaries of polycrystalline Si,[156] bands of dislocation loops,[157] cavities,[158] preexisting $a/c$ interfaces of small amorphous clusters,[135,159] or planar $a/c$ interfaces[98,147] have been observed to act as preferential nucleation sites for amorphization in Si irradiated at elevated temperatures.

The ion-beam-induced *c*-*a* transformation is critically dependent on the irradiation parameters. The kinetics of damage accumulation is controlled by a competition between

Downloaded 28 Oct 2008 to 192.84.153.250. Redistribution subject to AIP license or copyright; see http://jap.aip.org/jap/copyright.jsp

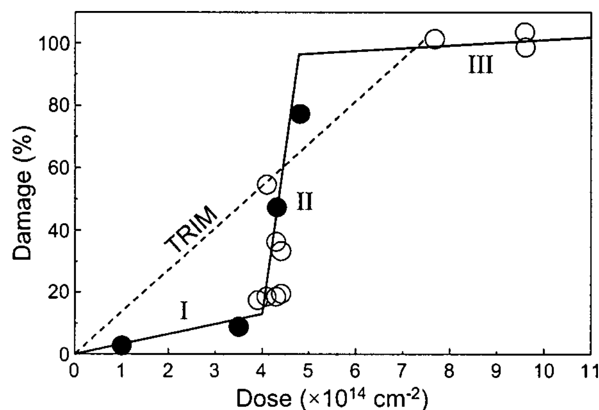


FIG. 9. Superlinear behavior of the damage vs dose for a 230 keV Si implant into Si(100) at room temperature. Symbols represent the maximum defect concentration as extracted from channeling spectra. The solid line is to highlight the trend. Regions I, II, and III can be clearly observed. The dashed line is the maximum value in the concentration profile of the Frenkel pair predicted by TRIM (from Ref. 93).

damage accumulation and dynamic annealing. The mass of the ion species, the temperature of the substrate, the dose and the dose rate of the irradiation all play an interdependent role.[108,160–162] It has been observed that damage in Si increases as the ion fluence increases. The implant dose at which a wholly amorphous layer first appears is referred to as the *threshold fluence* (dose). It was found that the threshold fluences required for light ions are much greater than those for heavy ones and that room temperature implantations require a much higher fluence than those carried out at liquid nitrogen temperatures.[107,109,112,148,163,164]

### A. Dose: superlinear damage accumulation

The damage level in Si characterized by different experimental techniques [IR spectrometry,[64,111] x-ray difraction,[93] and RBS (Ref. 99) ] indicates that during self-ion irradiation, the most damaged region shows an increased damage accumulation with three distinct regimes (see Fig. 9). Initially the damage $D$ grows slowly with a sublinear dependence on dose $\Phi$ until a critical dose is reached ( $D \propto \Phi^{\beta}$, $\beta < 1$, region I). Then, a rapid superlinear growth within a very narrow dose range occurs ( $D \propto \Phi^{\beta}$, $\beta > 1$, region II). And finally the damage saturates beyond a given dose (region III). Further implantation only causes the widening of the amorphous layer. Region I is associated to relative simple defects in *c*-Si, while the intermediate damage region II is likely to result from a mixture of damaged *c*-Si and *a*-Si zones. Region III is identified as amorphous material.[64,93,108]

Several attempts have been made to address this issue. Bai and Nicolet compared the experimental evaluation of the damage level with the Frenkel pair concentration provided by TRIM (dashed line in Fig. 9).[93] In the first region the experimental damage is significantly lower than that predicted theoretically. The initial sluggish increase of the damage is due to the considerable recombination of point defects at room temperature. In region II, the damage increases with dose much faster than the production of Frenkel pairs calculated from TRIM. The rapid growth of the defect concentration is attributed to the reduction of the threshold energy for atomic displacements in a predamaged crystal. The production rate of stable defects is thus proportional to the concentration of existing defects, and the effect of dose is no more simply additive.

Holland *et al.* explained this behavior assuming that during the initial sublinear regime damage consist of simple defects, predominantly of a vacancy character.[165] The onset of the superlinear growth was attributed to the nucleation of *a*-Si when the defect (divacancy) density exceeded a critical value. The presence of *a*-Si alters the balance between defect reactions and promotes the growth of divacancy damage which in turn leads to further amorphization. The ion-induced *c*-*a* phase transition in Si is then considered a cooperative process in which its onset triggers a rapid growth of the defects required for amorphization.

### B. Ion mass

The slope of the damage accumulation versus dose curve in region I increases with the increase of ion atomic number $Z_i$ and the onset of amorphization is shifted towards lower dose values.[111] For heavy ions, such as Sb (Ref. 111) and Sn (Ref. 64), no transition is observed between region I and II and a proportionality between the damage and the dose is found ($\beta = 1$).[112] As the ion mass increases, amorphization is possible with lower doses. While amorphization can be easily achieved with Sb at doses in the order of $10^{14}$ cm$^{-2}$, doses of at least $10^{16}$ cm$^{-2}$ are needed to form a continuous amorphous layer with B ions at room temperature.[144] The experimental measured dependence of the damage level with dose for several ions is shown in Fig. 10.

The effect of the ion mass is not surprising taking into account the variety of the damage generated by different ions. For the same implant energy, a larger fraction of the incident energy is used in nuclear collisions in the case of higher mass ions, thus causing more atomic displacements. The differences not only come from the amount of generated defects, but mostly because of the morphology of the produced damage strongly influences its dynamic anneal and therefore the rate of accumulation. Distinct behavior of the damage accumulation observed for similar ion masses, such it is the case of Si and P,[102] can be attributed to chemical effects of P which enhances the growth of induced damage, similar to what it is observed in SPEG.[67,70]

TEM studies[126] and MD simulations[125] show that heavy ions produce direct formation of amorphous regions from the ion impact, thus essentially undamaged crystalline and amorphous volumes are assumed to coexist. The *c*-*a* transformation is mainly due to the linear accumulation of amorphous regions. Whereas light ions, such as B, produce mostly isolated point defects or small defect clusters. Its accumulation is hindered by its rapid annihilation at room temperature and thus the dose required to cause the transformation from highly damaged *c*-Si to *a*-Si is higher and occurs superlinearly.[111] Contrary to the ordinary remark that *c*-Si cannot be rendered into *a*-Si by electron irradiation,[166] Takeda and Yamasaki found that *c*-Si can transform to *a*-Si under electron irradiation with doses of the order of $10^{22}$ cm$^{-2}$ if high electron energies ($>1$ MeV) and low tem-

Downloaded 28 Oct 2008 to 192.84.153.250. Redistribution subject to AIP license or copyright; see http://jap.aip.org/jap/copyright.jsp

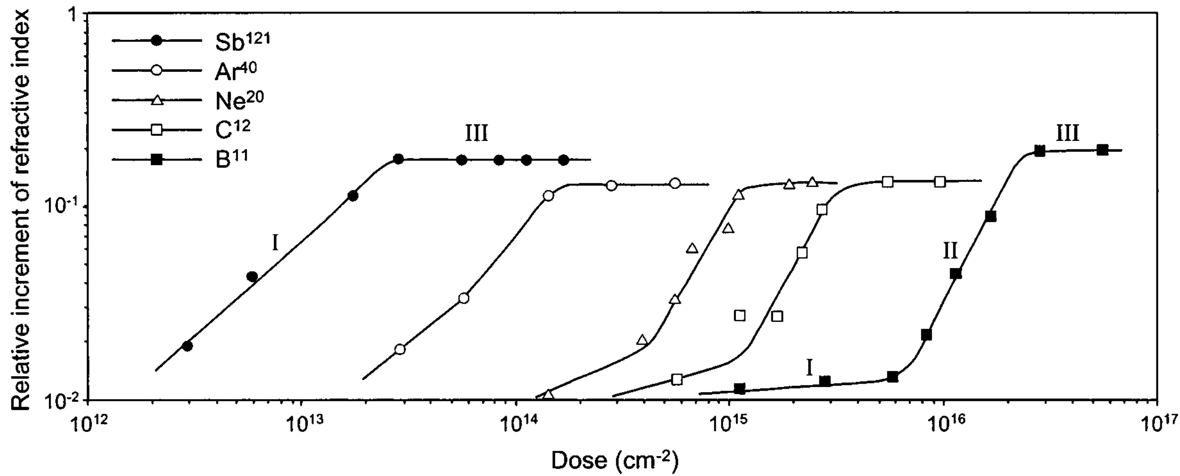


FIG. 10. Relative increment of the refractive index of Si as a function of the dose for 80 keV irradiations at room temperature with several ions. Regions I, II, and III are also observed (from Ref. 111).

peratures (25 K) are used.[167] High electron energies are required to produce atomic displacements and low temperatures to freeze the dilute damage produced by the irradiation and thus make possible the damage accumulation.

An interesting feature observed by Davies *et al.* is what they called *superadditivity*: the number of lattice Si atoms displaced by implantation of polyatomic-carbon-ion beams $C_n$, for several values of $n$, was found to increase superlinearly with $n$.[101] In other words, polyatomic ions cause more damage than the same ions implanted separately. The damage observed in the case of a single ion of atomic mass equivalent to $C_n$ was higher than that for $C_n$. This effect has also been observed for $BF_n$ and $PF_n$ molecular implantations, as shown in Fig. 11.[127] Howe and Rainville observed that the damage produced by a diatomic ion was always more resistive to annealing than that produced by the monoatomic ion of the same velocity.[126] The effect is higher than the one expected because of the larger initial average diameter of the damaged regions produced by a diatomic implant ($Bi_2$) compared to that for the corresponding monoatomic implant. The damage size is not only different but its morphology, and this seems to be a key factor in determining how much of the created damage is retained.

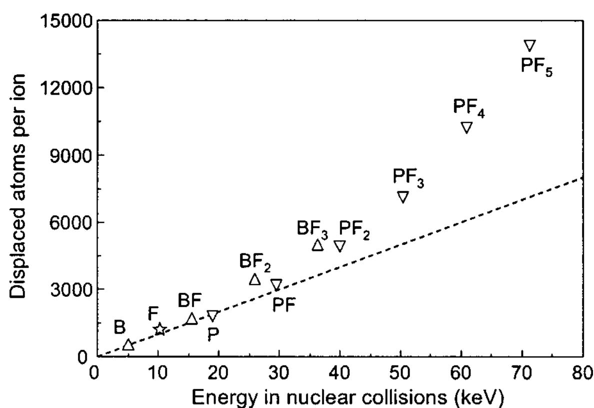


FIG. 11. Number of displaced atoms as measured with RBS *in situ* after implantation of B, F, P, $BF_n$ $(0 \leq n \leq 3)$, and $PF_n$ $(0 \leq n \leq 5)$ at 77 K. The number of displaced atoms increase more than linearly as indicated by the dashed line (from Ref. 127).

### C. Energy

The threshold dose is relatively insensitive to ion energy. This is not surprising since amorphization occurs near the end of range damage, i.e., when most of the implanted ions stop and have low energies. Dennis and Hale studied the energy dependence of the critical amorphizing dose in different conditions.[168] Using ESR they observed an increase of the critical dose with ion energy for a light ion (Li), almost no dependence for an intermediate ion (Ar), and a initial reduction of the critical dose with energy at low energies and then no energy dependence at higher energies for a heavy ion (Kr). These experimental findings are shown in Fig. 12. As the energy increases, the projected range also increases and consequently the ion energy distributes in a wider zone, keeping the deposited energy per unit length approximately constant. The different behavior is produced because for light ions electronic losses are higher than in the case of heavy ions, and thus a greater fraction of the total ion energy goes into electronic processes, while only nuclear collisions generates atomic displacements.

### D. Implant temperature: the critical regime

The threshold dose is a strong function of the implant temperature. For a given ion, the threshold dose increases as the temperature increases. The influence of irradiation temperature is stronger for light ions and higher temperatures. For a given dose, amorphization is not possible above a critical temperature, which increases with the increase of ion atomic number (see Fig. 13).[109,148,163,169] At low temperatures, the minimum dose for the formation of an amorphous layer increases with mass in a progressive way. For example, at $-170$ °C, the threshold dose for amorphization is $10^{15}$ cm$^{-2}$ for B implants, $2\times10^{14}$ cm$^{-2}$ for P implants, and $3\times10^{13}$ cm$^{-2}$ for Sb implants.[163] As the temperature increases it becomes more difficult to amorphize with lighter ions: at 30 °C, the threshold doses are $8\times10^{16}$, $6\times10^{14}$, and $10^{14}$ cm$^{-2}$ for B, P, and Sb implants, respectively. Above 130 °C no amorphization with B and P is observed, while with Sb is still possible to amorphize for doses of 5

Downloaded 28 Oct 2008 to 192.84.153.250. Redistribution subject to AIP license or copyright; see http://jap.aip.org/jap/copyright.jsp

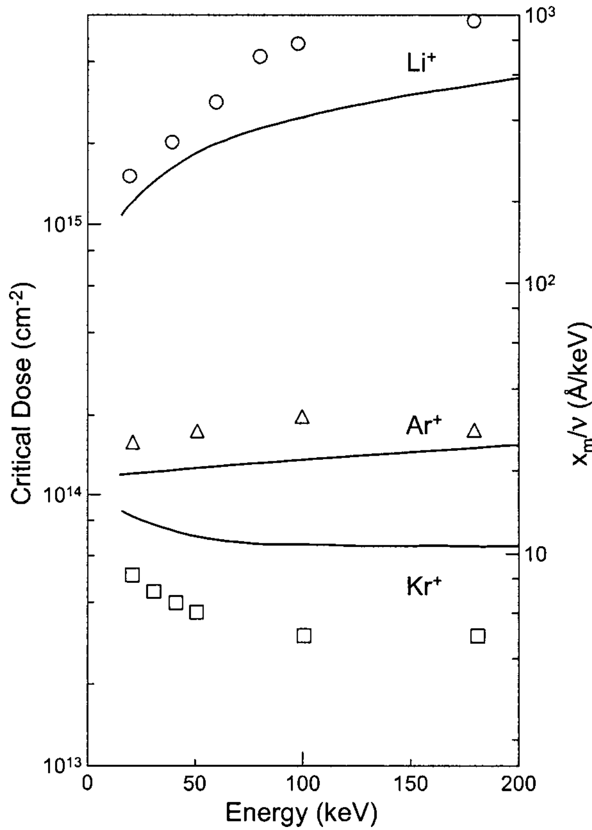


FIG. 12. Critical amorphizing dose as a function of the implantation energy for several ions at 80 K (from Ref. 168). Solid lines are theoretical curves assuming the critical energy density model (described in Sec. V A).

$\times 10^{14}$ cm$^{-2}$. The amorphization by electron irradiation is observed only at temperatures below 25 K.[167]

The reduction of implant temperature has similar effect to the increase in ion mass. At low implant temperatures,

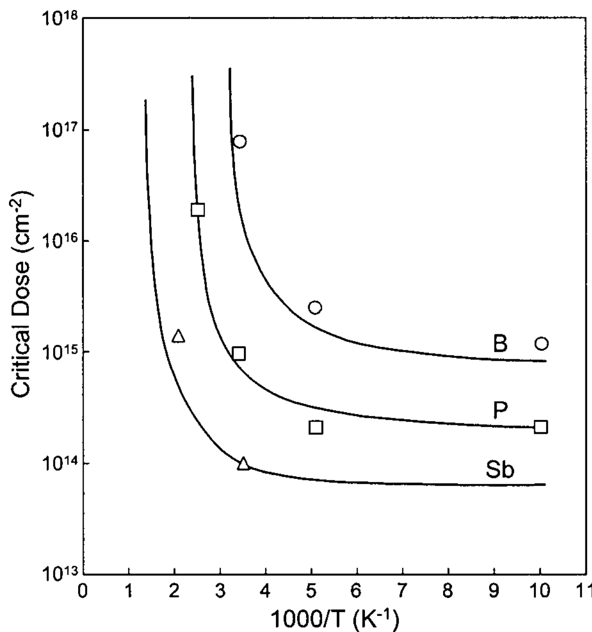


FIG. 13. Logarithmic plot of the critical dose for amorphization vs $1/T$ for several ion types. The temperature at which amorphization is possible at a given dose shifts to higher values as the ion mass increases (from Ref. 163).

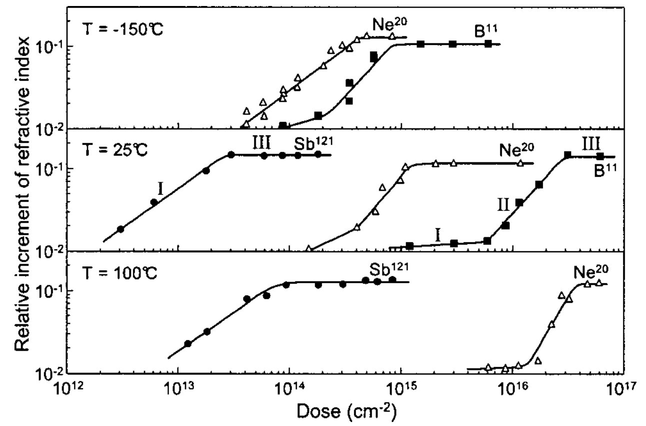


FIG. 14. Relative change of the refractive index vs dose for Si irradiated by Sb (Ref. 121), Ne (Ref. 20), and B (Ref. 11) ions at target temperatures of −150 °C, 25 °C and 100 °C (from Ref. 112).

amorphization can be achieved at lower doses and the region I and II (defined in Sec. IV A) are joined together into one region in which damage is proportional to the dose $\Phi$, as it occurs for heavy ions.[112] In the case of B and Ne at 25 and 100 °C, the curves have the three characteristic regions. In the case of Sb (at 25 and 100 °C) and Ne (at −150 °C) the curves of damage accumulation versus dose have regions I and III only. When increasing $T$, the damage curves are shifted toward the greater values of $\Phi$, the slope $\beta$ of region I decreases in the case of B and Ne. These experimental findings are shown in Fig. 14. The superlinear behavior can be observed for all ions in the appropriate temperature range.

The temperature dependence of ion-beam-induced amorphization is considered to be due to competition between defect accumulation in the energetic collision cascade and damage shrinking associated to defect annihilation or outdiffusion from the damaged region. For low implant temperatures most of the generated damage is retained and the damage rapidly increases with dose.

Under conditions where the rate of dynamic annealing closely balances the damage production rate, small changes in implant temperature, fluence, and flux can dramatically alter the level and nature of residual disorder.[164] Around the temperature at which the damage annihilates at the same rate as it is created, a slight increase in temperature favors the damage annihilation preventing amorphization. The extremely nonlinear damage accumulation with substrate temperature for irradiation of constant flux and fluence is indicative of a critical transition.[157] The critical temperatures for similar implant conditions are found to shift to higher values as the ion mass increases (see Fig. 13). For Si implants, this critical transition occurs near room temperature.[100] For this reason beam heating effects could lead to variable results under nominally "identical" conditions unless special care is taken to thermally couple the target wafer to a temperature-controlled holder.

For a constant current density irradiation in this regime, the dose required to form a buried amorphous layer by Si self-implantation increases steadily with temperature, at a rate of around $1.2 \times 10^{14}$ cm$^{-2}$ K$^{-1}$.[148,169] Thus, an increase in the implant temperature and hence in the dynamic defect

Downloaded 28 Oct 2008 to 192.84.153.250. Redistribution subject to AIP license or copyright; see http://jap.aip.org/jap/copyright.jsp

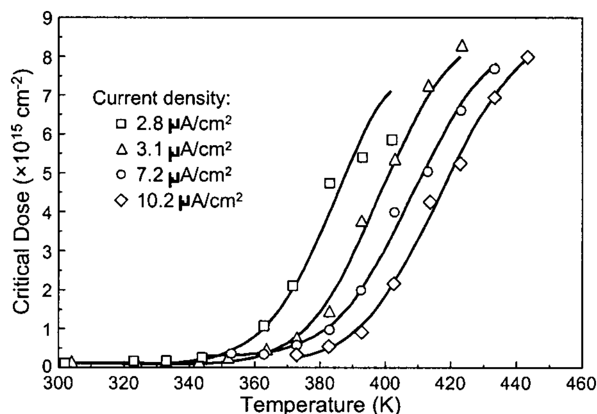


FIG. 15. The dose of 80 keV Si ions needed to produce a buried amorphous layer vs substrate temperature. Data are shown for several current densities (from Ref. 169).

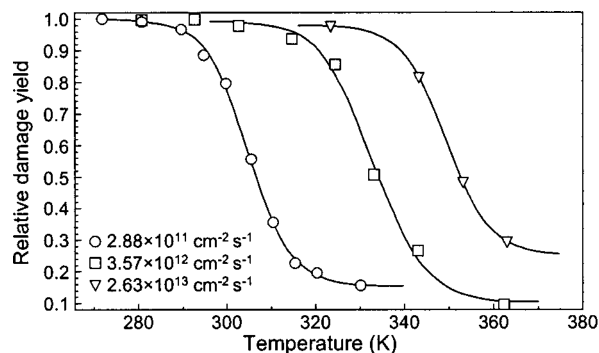


FIG. 16. Relative damage yield as a function of the Si substrate temperature for 1 MeV Si irratiations to a fixed fluence of $1\times10^{15}$ cm$^{-2}$ at several dose rates (from Ref. 100).

annealing rates, can be compensated for by increasing the irradiation dose (see Fig. 15). Alternatively, at a fixed amorphization dose a higher temperature regime is applicable for higher density currents.

### E. Dose rate

Holland *et al.* observed that for Si irradiations in Si at cryogenic temperatures there is no flux dependence in the amount of residual damage created.[170] However, for room temperature irradiations they observed that damage increased with increasing dose rate. At high dose rates, the predicted TRIM damage profile was similar to the one observed experimentally, while at lower dose rates the experimental profile was significantly lower. This behavior is understood in terms of the balance between damage generation and annihilation. At low temperatures no dose rate effect is observed because the annealing is negligible in the time range of practical dose rates. The critical temperature for Si implants is close to room temperature, therefore in this temperature range the annealing time (determined by the dose rate) will have a significant influence. As the dose rate increases, the time between the arrival of overlapping cascades decreases, thus resulting in increasing damage accumulation. However, for high implant doses, the amount of damage was observed to decrease slightly as the dose was increased.[170] This inverted dependence on dose rate for high doses is probably due to the temperature rise that occurred during the high flux implantation.

For a constant fluence irradiation a critical flux exist above which an amorphous layer is formed and below which the irradiated crystal contains only extended defects. Elliman *et al.* illustrated the effect of flux for different ion species by comparing the damage created by Ar and Xe implantations in Si.[148] The amorphous threshold flux is observed to be almost three orders of magnitude higher for Ar than for Xe, for constant fluence irradiations. Considering that the maximum nuclear stopping power is four times higher for Xe than for Ar, in principle, it should be possible to compensate for differences in the total number of displaced atoms by increasing the Ar fluence appropriately. Four times increase in the fluence is sufficient to account for differences in the total number of defects produced by Ar and Xe, but the amorphous threshold flux for Ar is still over an order of magnitude higher for Ar than for Xe. This suggests that the dynamical anneal within cascades and/or the cascade size are also important parameters.

The nucleation of a buried layer, under conditions where dynamic defect annealing is significant, depends heavily on the irradiation beam flux and substrate temperature. The combination of flux and temperature indicates how dynamic defect annealing and defect production (controlled by temperature and flux, respectively) can be balanced to control amorphization over a wide range of implant conditions.[148] The amorphous threshold flux was found to exhibit a strong temperature dependence (see Fig. 16). The critical temperature is found to increase with dose rate for the same bombardment dose, thus balancing the decrease in the annealing time with the increase in temperature.[100]

When plotting the point at which the disorder peak first reaches the random level at the end of range damage in Si, the temperature dependence of the amorphous flux satisfy an Arrhenius expression.[169] A series of apparent activation energies ranging from 0.7 to 1.7 eV were determined with ions ranging from 12 amu (C) to 132 amu (Xe), as can be seen in Fig. 17. If these energy values were associated to discrete defects, the different activation energies would require the existence of different defects controlling the *c*-*a* transition for each ion type. This seems unlikely because the structure of the damaged crystal, just before the onset of amorphization, is thought to be very similar in nature for all ion species.[169] It is more likely that several processes may be operative and that the activation energy is influenced by the differences in defect interactions which results from changes in the density of defects created in the collision cascades of the various ions and the temperature of the substrate. As the percentage of simple defect complexes changes with deposited energy density, one defect may become crucial in controlling defect concentrations and interactions. But at different temperatures other defects may be operative.

## V. MODELS FOR AMORPHIZATION

Various authors have investigated the mechanisms of the *c*-*a* transition and several models have been proposed to interpret the experimental results, although no single model

Downloaded 28 Oct 2008 to 192.84.153.250. Redistribution subject to AIP license or copyright; see http://jap.aip.org/jap/copyright.jsp

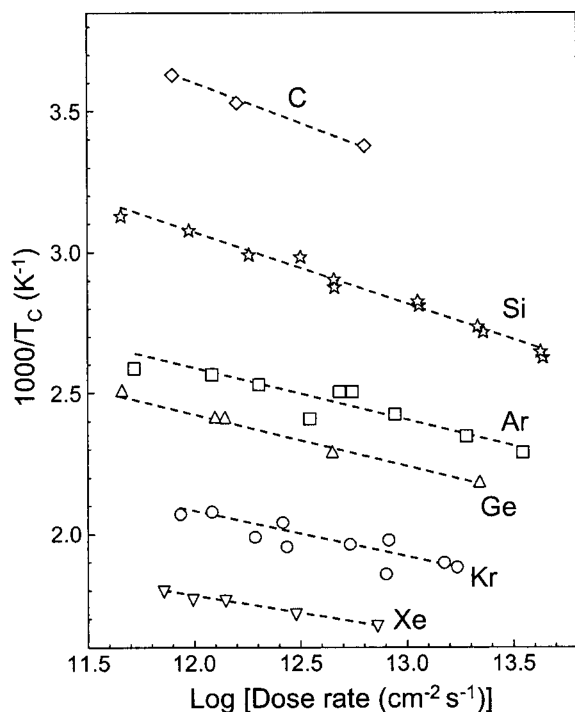


FIG. 17. Crystal-amorphous transition temperatures for (100) Si irradiated with 80 keV ions to a fluence of $1 \times 10^{15}$ cm$^{-2}$ using several ion types as a function of dose rate. The data points for carbon are for irradiations to $2 \times 10^{15}$ cm$^{-2}$ (from Ref. 169).

appears to properly account for all the experimental observations and few of them provide a quantitative approach. While some experiments indicate that the damage produced in the collision cascades consists mostly of point defects and small defect clusters suggesting homogeneous amorphization mechanisms, other observations evidence the presence of amorphous zones in the cascade tracks which is more congruous with heterogeneous amorphization models. In this section we will review the most significant phenomenological and structural models proposed to explain ion-beam-induced amorphization and thermal recrystallization in Si.

### A. Critical energy/defect density model

This model assumes that the *c*-*a* transformation is due to an increase in the lattice energy above a critical value.[107,171] This energy increase comes from the nuclear-stopping portion of the energy deposited by the implanted ions in their collisions with the lattice atoms as the implantation proceeds. When the deposited energy is high enough, it becomes energetically favorable for the defective lattice to transform into the amorphous state. Thus, the criterion used for amorphization in this model is that the energy deposition per unit volume exceeds the critical value, which has been given in the order of $5 \times 10^{23}$ eV/cm$^3$.[172–175]

When the implantation temperature is sufficiently low to suppress the effects of defect annealing and diffusion, the critical energy required for amorphization is not strongly dependent on the mass of implanted ions.[64,107,171,174,175] However, this value increases substantially with implantation temperature, especially for light ions. For room temperature implants, the critical energy is about a factor of 3–4 higher for Si and Sn implants and a factor of 20 for C compared to the value at liquid nitrogen temperatures.[64] The increase in the critical energy with implant temperature points up the self-annealing effects and defect diffusion which reduce the energy density stored in the defective lattice. Consequently, a higher deposited defect density is required to form an amorphous layer. The fact that the increase of the critical energy for higher temperatures is much larger for C than for Si and Sn is also consistent with the suggestion that the annealing rate of damage is dependent on the size and morphology of the damage.[113] Consequently, the critical energy value depends on implant parameters.

From the critical energy value, one could derive the required fluence for amorphization. At the critical dose the energy balance between the average energy density deposited into atomic processes and the critical energy density can be written as $\Phi\nu/x_m = E_c$, where $E_c$ is the critical energy density (eV/cm$^3$), $\Phi$ is the critical dose (ions/cm$^2$), $\nu$ is the energy deposited per ion into atomic processes, and $x_m$ is the depth of the damage (e.g., depth corresponding to 90% damage accumulation). Then $\nu/x_m$ is the energy deposited per unit length in the damaged region.[107] The maximum value of the energy deposited per unit length for a 380 keV incident particle energy is 147 eV/Å for Sn, 26 eV/Å for Si, and 7.6 eV/Å for C. Thus light ions having a lower deposited energy per unit length will result in a lower density of damage and will require a higher dose to reach the critical energy $E_c$ to induce amorphization.[64] The deposited energy density increases with increasing fluence until the damaged crystal is unstable with respect to the amorphous phase (the free energy of the defective crystalline phase exceeds that of the *a*-Si) and the *c*-*a* transformation occurs.

The deposited energy is responsible for atomic displacements or defects in the Si lattice. Thus, amorphization can also be envisioned as a phase transition induced by an accumulation of a critical defect concentration in *c*-Si.[171,176,177] Swanson *et al.* proposed as a criterion for amorphization that the defect concentration in the Si lattice exceeds 0.02 the atomic fraction.[176] The comparison of the positions of the *a*/*c* interfaces of an amorphous layer observed in TEM images with the damage estimated by TRIM simulations, indicates that amorphization occurs when the initial defect concentration exceeds a level of about $1.15 \times 10^{22}$ cm$^{-3}$.[37] When dynamic annealing effects are important (the ion flux is too low or the implant temperature is high) then the defect density is reduced compared to the values predicted by TRIM. An increase in the defect generation is needed to account for the additional annealing effects.[38,91]

This model is also known as *homogeneous amorphization mechanism*. According to it, *a*-Si is thought to nucleate as a result of an interaction among a sufficient number of defects, produced within different collision cascades and distributed homogeneously throughout the irradiated region. This model assumes that Frenkel defects formed within an ion cascade are long-living and outdiffuse from the cascade volume so that any spatial correlation with the cascade volume is lost prior to their interaction. For Holland *et al.* the defect accumulation is controlled by the divacancies,[165] while for Motooka *et al.* is the accumulation of divacancy

Downloaded 28 Oct 2008 to 192.84.153.250. Redistribution subject to AIP license or copyright; see http://jap.aip.org/jap/copyright.jsp

and di-interstitial pairs which gives rise to amorphization.[178,179]

This model is more appropriate to describe those cases where irradiation produces low density cascades and simple defects, as it happens with Si or light ions at room or higher temperature.[128,165,170,177] According to this model, the onset of amorphization is expected to occur only after an incubation period (during which damage levels increase to the critical concentration), and therefore the growth of the amorphous phase will occur abruptly over a narrow range in dose, accounting for the superlinear dependence.[165] The observation in XTEM of a sharp $a/c$ interface and the prevalence of crystalline images (confirmed by the diffraction pattern) in damaged regions or even near the $a/c$ interface until the amorphous transition occurs under Si irradiation, are also indications of an abrupt transformation associated to homogeneous amorphization.[128,136,179]

However, a number of observations suggest that amorphization cannot be caused only by point defect accumulation.[112,125,126] If this were the case, the critical dose for amorphization would be lower for lower mass ions since more isolated Frenkel pairs are produced in this case,[125] contrary to observations.[102] Heavier ions produce mostly defects in clusters or amorphous pockets, and these defects will represent the main contribution to Si amorphization in these cases. Baranova *et al.* suggested that the condition for homogeneous amorphization may not be sufficient: the region transforming to the amorphous state not only has to exceed a critical defect concentration value, but also a critical size $R_{cr}$.[112] Regions with large concentrations but size smaller than $R_{cr}$ can momentarily transform to the amorphous state but quickly recrystallize.

### B. Overlap damage model

In this model continuous amorphization of ion implanted Si is due to the overlapping of the locally amorphized regions around each ion path until a continuous amorphous layer is formed.[163] For less dense cascades, the overlap of a larger number of damage regions produced by different ions is needed to stimulate the phase change. Morehead and Crowder[163] analytically developed this idea assuming that the disordered core surrounding the ion track was cylindrical and vacancies, or primary defects in general, could escape via thermal diffusion (see Fig. 18). The ultimate stable radius of the amorphous region, $R_o - \delta R$, and hence the number required for them to overlap and form a continuous amorphous layer, depends both upon the original average size of the damage $R_o$ and the temperature-dependent outdiffusion of primary defects which reduce the size an amount $\delta R$. $R_o$ is determined by the energy lost by the projectile ion in nuclear displacements per unit length. The damage area per ion [proportional to $(R_o - \delta R)^2$] is larger for heavier ions because of higher nuclear energy loss per unit length (bigger $R_o$), and greater resistance to annealing effects (smaller $\delta R$). The stopping power is not strongly dependent on ion energy over a relatively wide range for most ions, so that ion energy is of

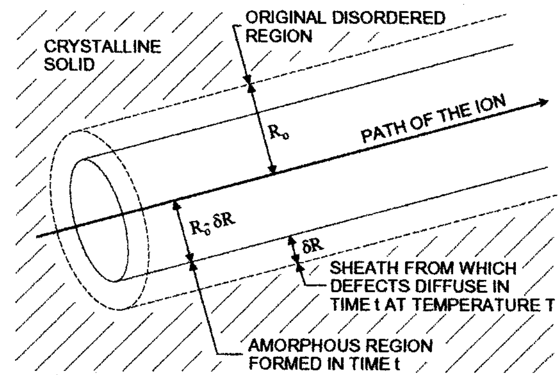


FIG. 18. The damaged region surrounding the path of a high energy ion in a crystalline solid idealized as a cylinder (dashed lines). Defects escape from the outer sheath and only the inner core (solid lines) becomes amorphous (from Ref. 163).

secondary importance and primarily determines the width of the amorphous layer and not the dose required to produce it.[168]

Following this idea, Gibbons derived the number of overlapping cascades $n$ required for the production of amorphous zones of area $A_A$ as

$$A_A = A_0\left[1 - \left(\sum_0^n \frac{(A_i\Phi)^k}{k!} e^{-A_i\Phi}\right)\right], \tag{5}$$

where $A_0$ is the total area being implanted, $A_i$ the damaged area produced by a single ion along its track, and $\Phi$ the dose.[90] In the case of heavy ion implants, such as Sn, amorphization results from ion impact directly and no overlap is necessary.[64] Light ions produce cascades of smaller sizes and thus require a larger number of overlaps. Low values of the number of overlapping cascades give rise to a linear behavior of the amorphous fraction versus dose, as observed for heavy ions, while large values (many overlapping cascades) are required to fit the superlinear behavior observed in light ion implantation at room temperature, as can be seen in Fig. 19.[64,93]

The overlapping cascade model is also called *heterogeneous amorphization mechanism* because it assumes that locally amorphous zones are generated heterogeneously by the incident ions within the collision cascade. When an ion impact causes a sufficiently high local-defect density (or deposited energy density) a small region can be rendered amorphous during the quench time of the cascade (i.e., the time needed for the energy to dissipate to surrounding regions). As ion fluence increases, these zones accumulate and overlap to form a continuous amorphous layer.[126,163,180–182]

Structural observations of heavy ion implants are consistent with the heterogeneous formation of an amorphous phase along a single ion track.[107,126,127,182] In particular, TEM studies on low dose Bi implants in Si showed the presence of small amorphous clusters embedded in a single-crystal matrix.[126] The damage morphology and the crystallization kinetics of the amorphous regions formed by Si irradiation at cryogenic temperatures also reveal the discrete nature of the collision cascade.[136,137] This behavior is attributed to a reduced diffusion of defects so that they maintain their spatial

Downloaded 28 Oct 2008 to 192.84.153.250. Redistribution subject to AIP license or copyright; see http://jap.aip.org/jap/copyright.jsp

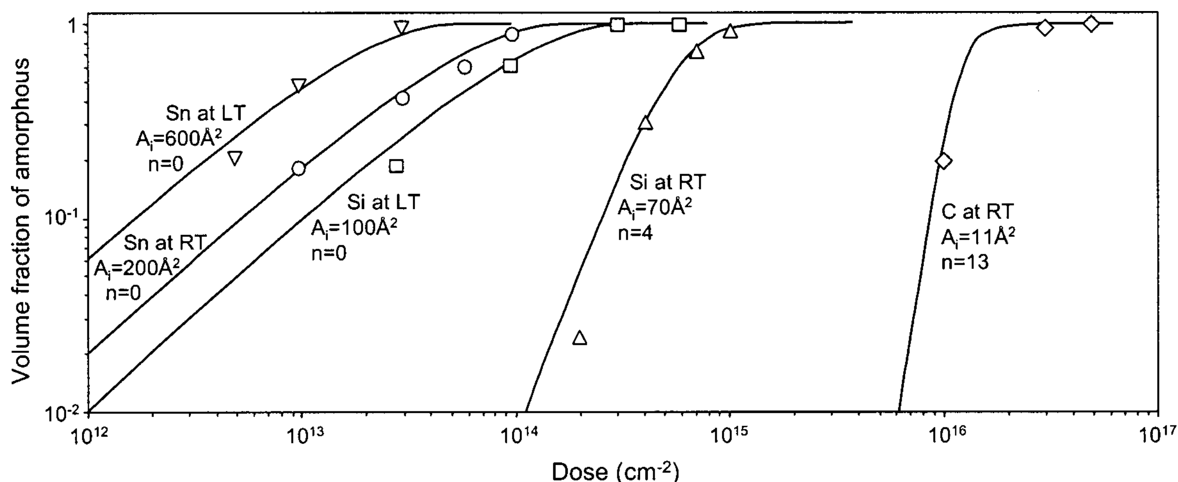


FIG. 19. Fraction of amorphous area vs dose for various ions, C, Si, and Sn, implanted at either room temperature (RT) or liquid nitrogen temperature (LT). Computer calculated curves from Eq. (5) are shown as solid lines with the corresponding parameters $A_i$ and $n$ (from Ref. 64).

correlation with the collision cascade volume after quenching, and any reaction between the defects occurs locally within the cascade volume.[128,136]

The effects of the dynamic anneal during high-temperature implants can be taken into account by the shrinking of the amorphous zones prior to overlap. According to this model, dose rate will be important only when it is high enough to yield a steady state concentration of primary defects in the crystalline material surrounding the disordered region which reduces the defect concentration gradient and retards their outdiffusion.

Some authors suggest that the two amorphization mechanisms, homogeneous and heterogeneous, could act simultaneously (a) gradual accumulation of local disordered crystalline regions and their sharp transition to the amorphous phase when the defect concentration reaches the critical value, and (b) direct formation of amorphous regions. Amorphization mechanism (a) would prevail for light ions, while for heavy ions amorphization arises mainly from mechanism (b).[107,111]

## C. Nucleation limited model

The facts that amorphization occurs preferentially at preexisting amorphous defects[135] or $a/c$ interfaces,[56,147,164] and that for a constant flux irradiation the fluence required to form a buried amorphous layer increases with temperature,[148] suggest that amorphization is consistent with a two-stage nucleation limited model, involving the production of suitable amorphization sites, via the accumulation of residual defects to reach a certain type or density, and the subsequent interaction of simple defects with these sites to produce the growth of the amorphous phase.

Campisano *et al.*[162] proposed that the kinetics of amorphous phase formation responds to a classical mechanism of nucleation and growth and that the process may be described by an Avrami-Johnson-Mehl equation for phase transformation:[183]

$$F = 1 - \exp(-K\Phi^n), \tag{6}$$

where $F$ is the amorphous fraction, $\Phi$ is the ion fluence, $n$ is an exponent which lies in the range 3–4 for three-dimensional growth, and $K$ is a temperature dependent parameter:

$$K = R_a V_a^{n-1}, \tag{7}$$

where $R_a$ is the nucleation rate and $V_a$ the growth velocity of the amorphous phase. The pure nucleation process can be ascribed to the prompt part of the collision cascade. Once amorphous islands are nucleated in the irradiated volume, the long-living ion-beam-generated defects interact with the interfaces between these islands and the crystal and can therefore induce their growth or shrinkage depending on the irradiation temperature and ion flux.

During the nucleation stage, defects remaining after the initial quenching of the damage cascade accumulate into complex defect structures and extended defects. Increasing in complexity with ion fluence, these residual defects accumulate until the free energy of the defected crystal reach a level that favors the nucleation of the amorphous phase. At this point, the nature of the residual defects is thought to be similar, regardless of the irradiating ion type.[169] Despite the applicability of a nucleation limited process of amorphization to a wide range of ion types and irradiation conditions, activation energies of the defect processes controlling EOR amorphization have been found to vary with irradiation conditions. It becomes evident that the activation energy is influenced by the differences in defect interactions which results from changes in either the cascade size, the irradiation temperature, or indeed, some combination of the two.

## D. Defect-based models

In order to provide models that describe amorphization and recrystallization processes at the atomistic level it is essential to identify the defects that can act as amorphous embryos, and those that induce recrystallization. It is generally believed that crystallization[153] and amorphization[162] under irradiation are related to each other and both processes are

Downloaded 28 Oct 2008 to 192.84.153.250. Redistribution subject to AIP license or copyright; see http://jap.aip.org/jap/copyright.jsp

generally ascribed to ion-beam-induced defects.[98] Because of the similarities between thermal and IBIEC (in both cases dopants produce a rate enhancement, and in both cases the growth along (100) orientation is faster than that along (111) orientation) it has been postulated that the same defect is responsible for both processes.[153] The differences in the activation energy could be due to the fact that the collision cascade generates the defect or provides the heat within the thermal spike needed to produce the transition.[98] Some authors consider that the recrystallization at the $a/c$ interface involve the generation and movement of defects.[147,152] Other authors suggest that the interfacial atomistic mechanisms responsible for recrystallization of *a*-Si occur through the breaking of bonds and network rearrangement.[184,185] In this section, several structure models are examined which identify particular types of defects with a relevant role in the amorphization and/or recrystallization mechanisms.

#### 1. Vacancies and vacancy complexes

Holmen *et al.* concluded that the energy deposited in nuclear collisions has a main influence on the ion-beam annealing process.[186] Since the vacancy concentration is related to the energy deposited in nuclear collisions by the ion beam, they considered that the diffusion of single vacancies toward the $a/c$ interface mediated crystallization.[149,186,187] Thompson *et al.* attributed the low-temperature annealing of damage clusters produced by heavy ion implantation in Si to the migration of divacancies from the core of the collision cascade.[134] Other authors proposed that the accumulation of divacancies at the $a/c$ interface led to amorphization.[147,148,188]

Linnros, Elliman, and Brown observed that the movement of an existing planar $a/c$ interface could be reversed depending on the temperature and dose rate of the ion implantation.[147,148] The dose rate at the reversal point follows an Arrhenius expression with an activation energy of 1.2 eV when irradiating Si with different ions.[147,148] Additionally, when scaling the results for different ions (by multiplying the dose rate by the square of the linear density of displacements produced along individual ion paths by each ion species), the data were found to lie on a universal curve for all the ions, with an activation energy of 1.2 eV. The quadratic dependence of the scaling on the linear displacement density at the interface suggests that a second-order defect complex, such as the divacancy, is of controlling importance.[147]

The fact that the derived activation energy for the balance between amorphization and crystallization at an existing planar $a/c$ interface[147] and for the onset of amorphization at the end of range[148] were both processes controlled by an activation energy of 1.2 eV, close to the reported activation energy for divacancy annealing,[188] suggested that the divacancy was the defect most likely to be controlling the transition to the amorphous phase, at least in the temperature range of 180–300 °C.[147] Furthermore, the Si divacancy anneals at temperatures about 200 °C, the same temperature range in which the equilibrium temperature (zero movement of the interface) typically lies. As a single activation energy could be ascribed to all of these processes, it was hypothesized that the same defect controlled the amorphization process in all cases. Later on, additional studies[100,169] showed that the measured activation energy for the onset of amorphization varied with ion mass and decreased for lower temperatures, suggesting that several defect-mediated processes may contribute to amorphization.

Holland[128] and Motooka[102] also supported the idea of divacancies having an important role on the amorphization process, through the interaction with other defects. According to Holland, damage accumulation is the result of reactions between simple defects (interstitial+vacancy, vacancy+vacancy, and divacancy+interstitial). The formation of amorphous regions or the existence of interfaces or extended defects that may act as a preferential sinking of interstitial type defects, could alter the balance between these simple reactions and promote the growth of divacancy damage in the surrounding regions. An accumulation of these defects increases the free energy of the crystal and finally the *c*-*a* phase transition occurs. Chemical rate equations were used in the model to express the relation between the dominant defects within the irradiated volume. However, no values to the parameters were given to extract quantitative understanding of the growth behavior of defect populations.[99,128]

Structural models at the atomistic level try to identify structures that contain five- and seven-membered rings, characteristic of the amorphous phase. Based on this criterion, Chadi and Chang questioned the role of vacancy clusters on amorphization because they are unlikely to contain odd-membered rings in their structures.[189]

#### 2. Self-interstitial clusters

Seidman *et al.* suggested the clusters of self-interstitials as amorphous embryos because they introduce the five- and seven-membered rings.[166] These authors postulated that the minimum stable amorphous embryo consists of a di-interstitial, so that the addition of a vacancy to an amorphous embryo produces a mobile self-intestitial. When the size of an amorphous embryo exceeds a critical value, it becomes an amorphous nucleus, i.e., a certain amount of material has become *a*-Si.

Based on the experimental data of amorphization during high-energy low-temperature electron irradiation, Takeda and Yamasaki also supported the role of the Si-self interstitials clusters in amorphization.[167,190] They suggested that the smallest cascade damage that could act as an *a*-Si embryo consisted of a cluster of four self-interstitial atoms.[92] The defect, which is shown in Fig. 20, consists of five-, six-, and seven-membered atom rings without any dangling bond. Other interstitial structures one can think of are apparently unstable, as the distortions of bond lengths and angles are too large to form actual covalent bonds.[191]

#### 3. Divacancies and di-interstitial pairs

Motooka[178] developed a model for the amorphization process in ion implanted Si based on the accumulation of divacancy and di-interstitial ($D$-$D$) pairs (see Fig. 21). In this

Downloaded 28 Oct 2008 to 192.84.153.250. Redistribution subject to AIP license or copyright; see http://jap.aip.org/jap/copyright.jsp

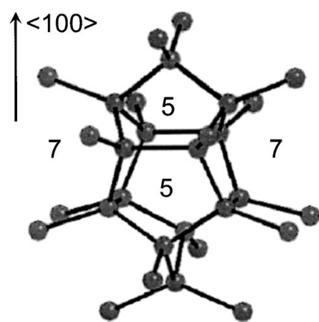


FIG. 20. Atomic structure of the cluster formed by four Si self-interstitials which has been considered as the amorphous embryo in electron irradiation experiments. It introduces in the lattice the typical five- and seven-membered rings of the amorphous phase (from Ref. 190).

model, the combination of a divacancy with a di-interstitial in the *c*-Si lattice results in a local atomic configuration including five- and seven-membered rings.

The atomic configurations obtained by the *D-D* pair model reproduce well the high-resolution images of the ion-beam-induced damaged layers.[91] Based on the proposed *D-D* model, radial distribution functions, bond-angle distributions, and phonon density of states were calculated as functions of the number of the *D-D* pairs and it was found, by comparing with experimental results, that complete amorphization occurs when the number of *D-D* pairs per atom exceed 0.2 or approximately two *D-D* pairs are introduced in the fcc cubic lattice.[192,193]

#### 4. IV pair or bond defect

Another defect that has also been proposed to be responsible for amorphization in Si is the so-called *IV pair*. Tang and co-workers encountered this defect when studying self-diffusion and interstitial-vacancy recombination in Si using tight-binding (TB) simulation techniques.[194] They found that when a vacancy approaches a ⟨110⟩ dumbbell interstitial, a metastable defect structure is generated instead of immediate interstitial-vacancy recombination. The defect consists of a local rearrangement of bonds in the crystal with no excess or deficit of atoms, and hence it is also known as *bond defect*. Its atomic structure is represented in Fig. 22, and the corresponding bond lengths and formation energy calculated using different simulation techniques in Table II. As can be seen, it introduces in the Si lattice the five- and seven-membered rings typical of the amorphous phase while maintaining perfect fourfold coordination. Tang *et al.* also studied the stability of the defect, showing that its lifetime could be in the range of hours at room temperature. This defect was also studied by Cargnoni *et al.* using *ab initio* Hartree-Fock calculations.[195] They showed that the IV pair consists of a large nuclear distortion compensated by electron charge rearrangement, and confirmed its stability. In both studies it was shown that its formation energy is comparable or even lower than the corresponding to the typical point defects in Si. Its equilibrium concentration should then be comparable or even larger than that of the other defects. However, the IV pair has not yet been detected experimentally, maybe because perfect fourfold coordination (which means no unpaired electrons) precludes its detection in standard experiments such as electronic paramagnetic resonance and electron nuclear double resonance. It has also been shown by first-principle techniques that the IV pair hardly disturbs the band structure of Si, which makes it undetectable in the deep level transient spectroscopy technique.[196]

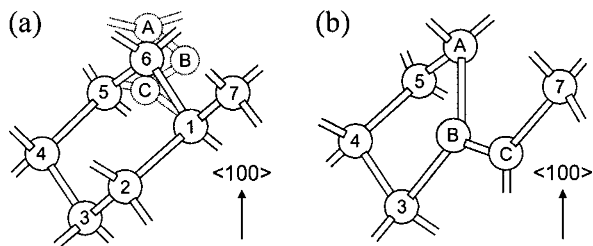


FIG. 21. (a) Basic structural unit for *c*-Si showing the six-membered ring. A ⟨100⟩-split di-interstitial is shown by the dotted line and the atomic sites *A*, *B*, and *C*. (b) Local atomic rearrangement after introducing a *D-D* pair. Atomic sites 3, 4, 5, *A* and *B* form a five-membered ring and 3, *B*, and *C* give a part of a seven-membered ring (from Ref. 178).

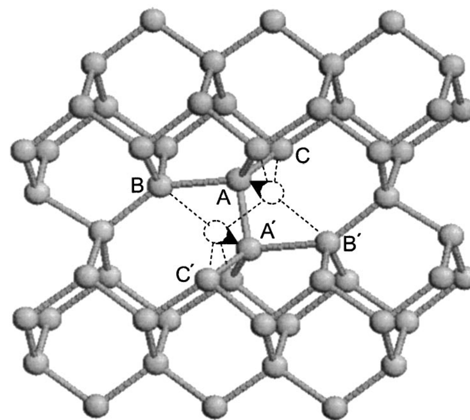


FIG. 22. Atomic structure of the IV pair. Dashed lines represent atoms and bonds in the perfect lattice. Atoms *A* and *A′* move along the directions indicated by the arrows and switch their bonds with atoms *B* and *B′*, giving rise to the IV pair. Bond lengths involved in the defect are displayed in Table II.

Using MD techniques, Stock and co-workers observed that the bond defect can be generated not only by incomplete interstitial-vacancy recombination, but also as a result of a pure ballistic process.[197] Thus the IV pair can be a primary defect generated by irradiation, with no need of preexisting interstitials and vacancies in the lattice for its formation. They showed as well that the IV pair is a characteristic structural feature of the *a*-Si/(001)Si interface.[197,198] Ishimaru *et al.* also observed this defect, combined with vacancies, in their simulation studies of the liquid-crystal transformation in Si.[199] Besides, it has been shown to form very stable structures when combined with Si self-interstitials.[200]

It is worth noting that the WWW model, the *D-D* pair of Motooka and the IV pair of Tang *et al.* introduce topological disorder in the Si crystal lattice in the same way, i.e., by switching bonds among neighboring atoms, but the final obtained structures are different.[197] It has been shown that *D-D* pair[178] and IV pair[200] accumulation leads to a volume expansion and to the presence of dangling bonds, while the WWW model predicts a volume contraction and perfect fourfold coordination.[47]

Downloaded 28 Oct 2008 to 192.84.153.250. Redistribution subject to AIP license or copyright; see http://jap.aip.org/jap/copyright.jsp

TABLE II. Lengths of the bonds involved in the IV pair and its formation energy, as obtained by using different simulation techniques: TB from Ref. 194, *ab initio* from Ref. 195, and classical MD using the Tersoff 3 potential (Ref. 201) from Ref. 200. Bond notation corresponds to that shown in Fig. 22.

| | TB | *Ab initio* | Tersoff 3 |
|---|---|---|---|
| $A-A'$ bond length (Å) | 2.28 | 2.27 | 2.28 |
| $A-B$ bond length (Å) | 2.46 | 2.46 | 2.51 |
| $A-C$ bond length (Å) | 2.38 | 2.39 | 2.35 |
| Formation energy (eV) | 3.51 | 3.26 | 3.01 |

#### *5. Dangling bonds*

By analyzing the temperature and flux dependence of the movement of a planar $a/c$ interface under ion irradiation, Jackson proposed a model based on the assumption that each ion creates damage that promotes amorphization, and at the same time creates defects that provide atomic mobility at the $a/c$ interface thus favoring crystallization.[152] From the experimental data of Linnros *et al.*,[147] Jackson concluded that the defects controlling ion-induced crystallization annihilated each other in pairs, and the defect migration energy was 1.2 eV. He suggested that this defect was a dangling bond in the amorphous phase, which moves around the interface region, rearranging the amorphous structure into the crystalline structure. The residual interstitials and vacancies generated in the crystal by the ions diffuse to the interface and get trapped there, thus promoting disorder and the growth of the amorphous phase.

#### *6. Kinks on terraces*

Based on atomic density and bonding arguments Csepregi *et al.* suggested that the regrowth interface is resolved into minimum-free-energy {111} planes or terraces during regrowth and that crystallization occurs via the propagation of [110] ledges on this terraced interface structure.[9] Spaepen and Turnbull[184] further developed this minimum-interfacial-free-energy argument and concluded that the interface should be highly saturated (i.e., with few unbonded atoms). Regrowth proceeds via a bond-breaking process and a subsequent rearrangement along the [110] ledges which form on this terraced interface structure. The bond-breaking event is responsible for the observed activation energy for the regrowth. Since the number of [110] ledges on {111} oriented terraces strongly depends on crystal orientation, this description is able to qualitatively explain the orientation dependence observed in conventional thermal annealing.[9]

Williams and Elliman extended this phenomenological model and assumed that the same kind of terraced structure is present in an $a/c$ interface, which is fully coordinated.[76] The defect (or "growth site") responsible for recrystallization is proposed to be a kink along a [110] ledge (see Fig. 23). Amorphous atoms at a kink site, unlike other atoms at the $a/c$ interface, have at least two bonds with the crystalline phase. This position is therefore the most favorable for the occurrence of recrystallization which proceeds via a kink motion along the [110] ledges. Kink nucleation and motion represent the basic step for the regrowth and require an activation energy of 2.7 eV. In nonplanar $a/c$ interfaces or the irregular interfaces of amorphous pockets, kinks and other growth sites can be already present at the boundary and should not be nucleated, thus resulting in low-temperature reordering.[135,137] As soon as the favorable configurations are completely crystallized and the interface sharpens up, low-temperature reordering is halted. Crystallization can then proceed only by a further increase in the annealing temperature which stimulates the nucleation of new kinks.[138] IBIEC of continuous amorphous layers has also been interpreted by Priolo and Rimini in terms of a kinklike motion along $[\bar{1}10]$ ledges at the $a/c$ interface.[98] According to these authors, ion implantation enhances crystallization because these kinks can be thermally generated within the thermal spike regime of the collision cascade.

## VI. ATOMISTIC CHARACTERIZATION OF THE AMORPHIZATION PROCESS

In this section we will introduce a fully atomistic model that we have developed on the basis of the IV pair as the fundamental building block to describe the amorphous phase. The ideas behind the model are based on MD simulations that characterize the IV pair properties as well as the interactions among these defects to give rise to more complex structures. The model is implemented in a kinetic Monte Carlo (kMC) code in order to simulate times and sizes directly comparable with experiments. As we shall see, it successfully reproduces the main experimental observations at the same time that provides detailed physical understanding of the amorphization and recrystallization processes in Si.

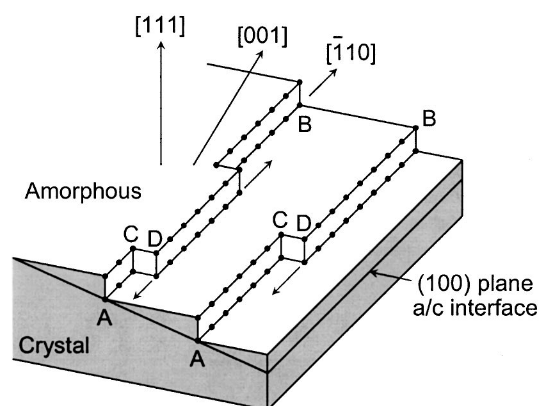


FIG. 23. Kinklike steps at the $a/c$ interface. The lower part of the figure (gray) represents crystal, while the upper part is amorphous. The (001) $a/c$ interface is composed of {111} oriented terraces; along the [110] ledges $(AB)$, presenton this terraced structure, kink steps $(CD)$ form. The motion of these kinks (indicated by arrows) produces crystallization (from Ref. 153).

Downloaded 28 Oct 2008 to 192.84.153.250. Redistribution subject to AIP license or copyright; see http://jap.aip.org/jap/copyright.jsp

### A. Molecular dynamics simulations

The MD technique consists in the numerical resolution of the classical equations of motion for a system of particles.[95] It provides a detailed description of the system dynamics at the atomic level, and thus it is a powerful tool that can be readily employed to explore the underlying physical mechanisms involved in the amorphization and recrystallization processes. In this type of simulation, the dynamics of the system is determined by the interatomic potential that describe the forces among atoms. It would be desirable to use first-principles or TB methods to get the forces, but unfortunately these calculations are very computationally demanding and are thus limited to systems of relatively few particles and very short total simulation times. In amorphization and recrystallization studies, even though no large systems are needed, simulation times are long in order to account for thermal annealing effects. It is then necessary to resort to the use of empirical interatomic potentials which are much less computationally intensive. Among the different potentials developed for Si, we have chosen to use the Tersoff potential within its third parametrization (T3),[201] since it gives a very good description of the Si amorphous phase.[202] Besides, the T3 potential has been successfully used to study the liquid phase of Si and its direct transformation to *a*-Si upon quenching,[203] the crystal growth from the amorphous phase[204] and the melt,[199] as well as several phenomena related to ion irradiation in Si.[205–207] The only limitation of the T3 potential is that the predicted crystal melting temperature, 2400 K,[200] is well above the experimental value, 1685 K.[208] However, this is not a serious drawback since it is possible to make a temperature rescaling between Tersoff temperatures and real temperatures.[209]

#### 1. IV pair structure and stability

The IV pair configurational and energetic properties predicted by the T3 potential[200] are in good agreement with TB (Ref. 194 ) and *ab initio*[195] results, as it is shown in Table II. However, some discrepancy was found when studying the IV pair stability, or in other words, its characteristic lifetime before annihilation. It has been shown that the IV pair always annihilates by the reverse movement of atoms $A$ and $A'$ of Fig. 22 toward the perfect lattice positions, switching again their bonds with atoms $B$ and $B'$.[194,200] IV pair annihilation never leads to the emission of the Si-self-interstitial and the vacancy. Using classical MD simulations with the T3 potential, the IV pair lifetime was shown to follow an Arrhenius behavior over a wide temperature range with an activation energy of 0.43 eV.[200] This value appears rather low in comparison with the 1.23 eV obtained from TB calculations[194] and the 1.32 eV from *ab initio*[195] methods. The discrepancy can be explained taking into account that the scheme followed in TB and *ab initio* calculations was a static relaxation procedure where symmetry in the IV pair annihilation path was enforced. Doing a similar calculation with the T3 potential, a higher value for the barrier, 1.05 eV, was found.[200] This is because when the system is allowed to freely evolve at a finite temperature, the IV pair annihilation sequence can differ from the symmetric path, and thus find another one with a lower energy barrier. The assumption of annihilating paths *a priori* is not needed in classical MD simulations since it is possible to obtain directly the recombination times.

The difference in activation energy values for IV pair annihilation implies a lifetime of only 3 $\mu$s at room temperature instead of several hours, as originally estimated by Tang *et al.*[194] Consequently, the IV pair as an individual defect is not stable enough to promote amorphization, since 3 $\mu$s is a very short time in comparison with the characteristic intercascade time at typical dose rates.

#### 2. Amorphization by IV pair accumulation

We observed that the stability of the IV pair increases when other IV pairs are present in the Si lattice.[200] In Fig. 24 we show the time evolution at different temperatures of the mean potential energy per atom in crystal lattices where several concentrations of IV pairs are introduced. Energy levels corresponding to *a*-Si, $E_{AM}$, and to *c*-Si, $E_C$, are also shown. As can be seen, mean potential energies in lattices with starting concentrations of 10% and 20% of IV pairs decreased to the value corresponding to the perfect crystal for all the simulated temperatures. This indicates that fully recrystallization occurred. However, in the case of the sample with 30% of IV pairs the mean potential energy decreases only to the $E_{AM}$ level, for all the simulated temperatures. In Fig. 25 we represent the radial distribution functions $g(r)$ corresponding to a pure amorphous matrix and to the lattice after introducing 30% of IV pairs, both thermalized at 1000 K. As can be seen, the radial distribution functions are very similar, indicating that structurally both samples are identical.

It is interesting to note that the behavior of the lattice with an initial IV pair concentration of 25% depends on temperature. For $T=1000$ K it returns to the perfect crystal, though initially the potential energy per atom is higher than $E_{AM}$, while it amorphizes for $T=1600$ K and $T=2000$ K. After introducing 25% of IV pairs, there are some traces of crystallinity left which act as a seed for crystal recovery at 1000 K, but further thermal agitation at $T=1600$ K and above dissolves these tracesand amorphization takes place. These findings are in agreement with the classical theory of nucleation and growth.[79] In the case of microcrystals of spherical shape embedded in the amorphous matrix, this theory predicts that there exists a critical radius $r_C$ given by

$$r_C = \frac{2\sigma}{\rho \Delta g}, \tag{8}$$

where $\sigma$ is the interfacial free energy per unit area, $\rho$ the atomic density and $\Delta g$ the free-energy difference between *a*-Si and *c*-Si in a per atom basis. $\Delta g$ is positive due to the lower free-energy content of the crystal. $\sigma$ represents the free energy necessary to maintain an interface between the crystalline and amorphous states and is also positive. Microcrystals having a radius larger than $r_C$ tend to grow spontaneously, and shrink otherwise. With increasing temperature the free-energy difference between amorphous and crystal $\Delta g$ diminishes, and consequently $r_C$ increases. This is probably the reason why at 1000 K the lattice with 25% of IV pairs

Downloaded 28 Oct 2008 to 192.84.153.250. Redistribution subject to AIP license or copyright; see http://jap.aip.org/jap/copyright.jsp

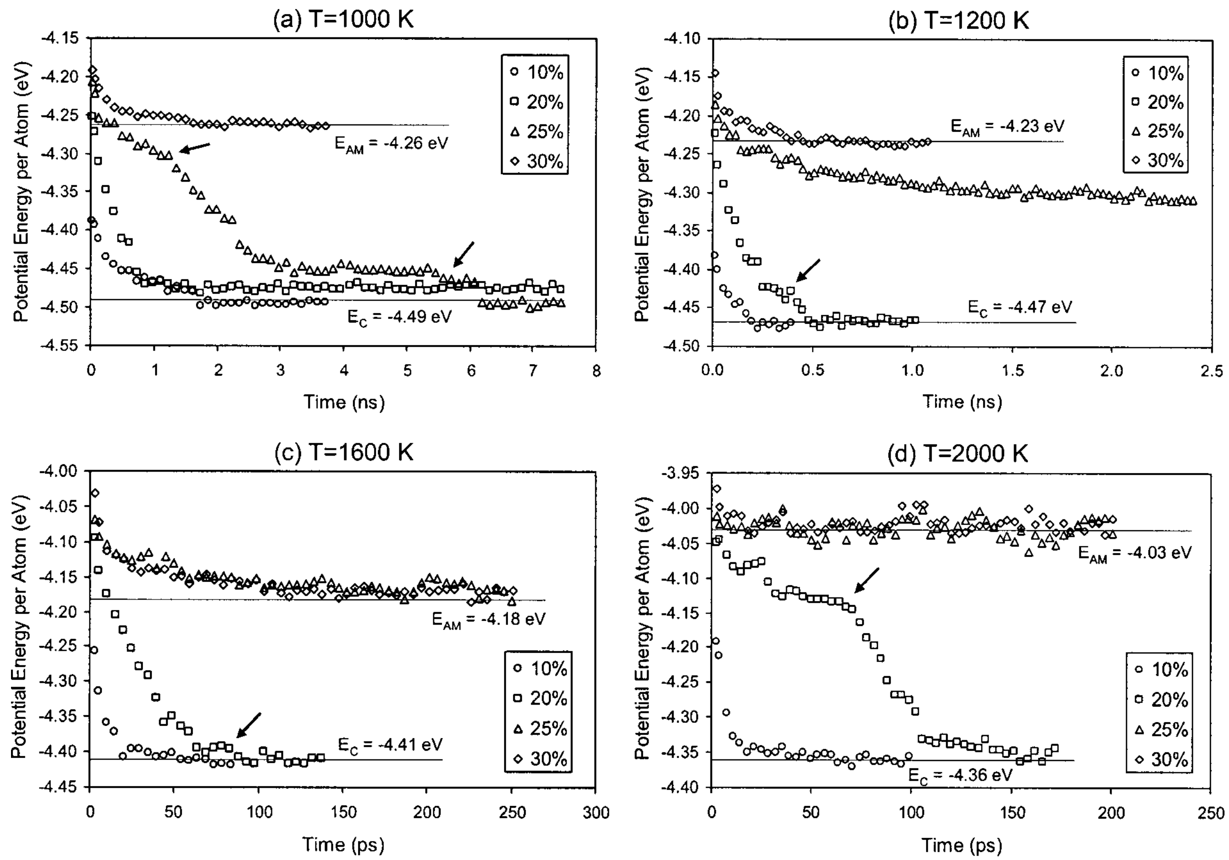


FIG. 24. Time evolution of the potential energy per atom in lattice samples with 10%, 20%, 25%, and 30% of IV pairs during the annealing at different temperatures. Solid lines indicate the mean potential energy per atom in *a*-Si and *c*-Si at each temperature, $E_{AM}$ and $E_C$, respectively. Arrows indicate plateaus followed by steep decreases, due to the more stable structures formed by the interaction of several IV pairs.

recrystallizes and at 1600 K and above amorphizes. Temperature then plays an important role in the amorphization process. Higher temperatures favor the recombination of the defects produced during the irradiation, and thus prevent the damage accumulation. But our simulations show that if the defects have accumulated and are interacting strongly, higher temperatures favor the amorphization. On the other hand, for the case of $T=1200$ K, the potential energy per atom stays between the levels corresponding to *a*-Si and *c*-Si. In this simulation the sample with a IV pair concentration of 25% started to recrystallize, but with a small misorientation with respect to the original perfect lattice due to thermal agitation. In real Si such a situation would correspond to the formation of low-angle grain boundaries, as it has been experimentally observed.[210,211]

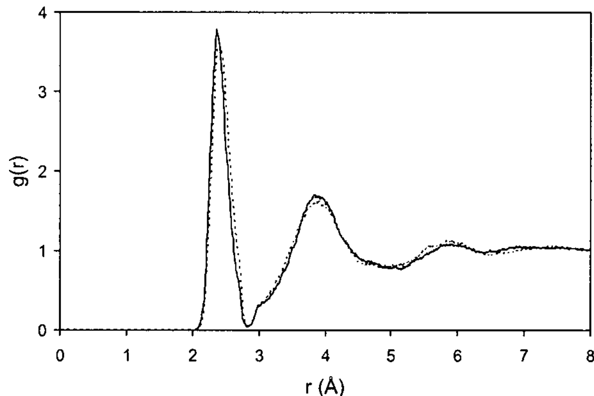


FIG. 25. Radial distribution functions $g(r)$ corresponding to a Si lattice with an IV pair concentration of 30% (solid line) and to a pure amorphous matrix (dotted line), both thermalized at 1000 K.

As can be deduced from Fig. 24, the higher the temperature, the higher the recrystallization velocity for the same concentration of IV pairs. For lattices with a concentration of 10% the energy decay is exponential, which suggests a single activation energy. Effectively, we observed that decay times in these cases followed an Arrhenius behavior with an activation energy of 0.45 eV, very close to the barrier obtained for IV pair recombination. This means that 10% is a concentration so low that IV pairs do not interact strongly with each other. They recombine one by one, and the overall crystallization behavior is the same as when there is just one IV pair. On the other hand, for higher concentrations the evolution of the potential energy per atom shows plateaus followed by steep decreases, indicated by arrows in Fig. 24. This behavior has been also observed in MD studies[125] and experiments[140] on the recrystallization kinetics of amorphous pockets created by ion irradiation. In these cases, IV pairs interact with each other and form more stable structures, responsible for the plateaus in the curves of Fig. 24. Recrystallization then requires the collective movement of several atoms which produces a sudden decrease in the potential energy per atom.

These MD simulations have proved that when IV pairs are present in the Si lattice to a given concentration

Downloaded 28 Oct 2008 to 192.84.153.250. Redistribution subject to AIP license or copyright; see http://jap.aip.org/jap/copyright.jsp

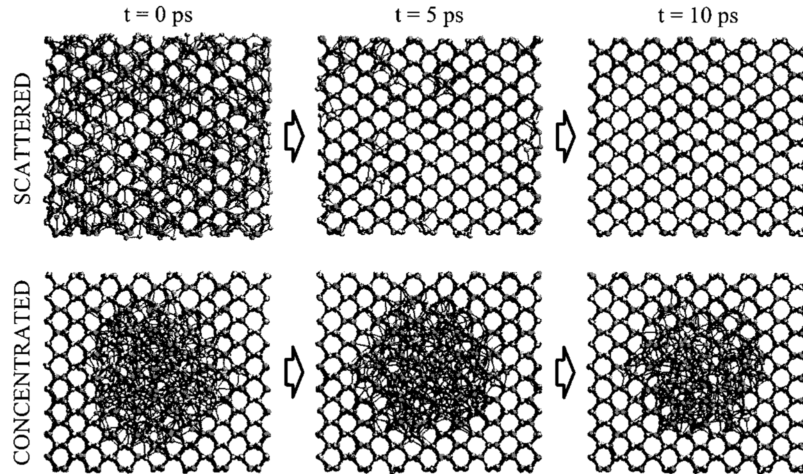


FIG. 26. Snapshots taken during the annealing at 1200 K of samples with the same amount of IV pairs (8%), scattered in one case and concentrated in the other. Each IV pair is introduced in the lattice by randomly choosing two neighboring atoms and displacing them as shown in Fig. 22. The scattered damage has disappeared after 10 ps of annealing, while the concentrated damage has barely shrunk.

(≃25%), amorphization of the Si lattice takes place. The resulting structure is identical to that corresponding to a pure *a*-Si matrix. Besides, the amorphous zones created by IV pair accumulation and those by direct irradiation showed the same features, as far as energy content, internal structure, density, and recrystallization dynamics are concerned. All these results indicate that amorphization can be achieved without the intervention of any additional defect, and also that amorphous pocket characterization can be studied by IV pair accumulation.

### 3. Influence of the damage morphology

IV pair accumulation serves then as a controlled way to introduce damage in the Si lattice. In this manner it is possible to generate amorphous pockets with a predefined geometry, so it is feasible to study the influence of its morphology on the recrystallization behavior. To get some insight on this last question, we carried out additional MD simulations at several temperatures in lattice samples with a IV pair concentration of 8%.[212] In one set of simulations IV pairs were distributed randomly in the lattice, separated from each other by a distance of at least 4 Å. In other set of simulations IV pairs were arranged in a sphere with a radius of 12 Å. The first set of simulations with scattered IV pairs would represent damage generated by electron irradiation or light ion implantation, while the second set with concentrated IV pairs would represent damage generated by heavy ion implantation (see Fig. 7).

Figure 26 shows several snapshots taken during the annealing of the two types of samples at 1200 K. After a simulated time of 10 ps, the scattered damage has disappeared completely, while the concentrated damage still remains. Even though the amount of IV pairs was the same, the dynamics of the recrystallization process is different. This result indicates again that when IV pairs are close to each other, they interact strongly forming more extended defect clusters whose lifetime is higher, and that the rate of IV pair recombination depends not on the global IV pair concentration, but on the local number of surrounding IV pairs.

In Fig. 27 we show the recrystallization velocities for both types of samples as a function of temperature. As can be seen, they show Arrhenius behavior over a wide temperature range, with corresponding activation energies of 0.44 and 0.89 eV for the scattered and concentrated damage, respectively. The obtained activation energy for the scattered damage is very close to that corresponding to isolated IV pair recombination, 0.43 eV. This indicates that the separation of 4 Å among IV pairs was long enough to prevent their interaction. In the case of the concentrated damage the activation energy is higher, and thus the recrystallization dynamics slower. Recrystallization starts from the $a/c$ interface, as it is also observed in experiments.[9,135] This is because IV pairs in contact with crystalline atoms are less stable than IV pairs near the center of the sphere. However, their strong interaction with IV pairs in the amorphous side of the interface make them more stable than if they were isolated. This cooperative effect is increased in the case of a planar $a/c$ interface, whose recrystallization velocity is also represented in Fig. 27. It shows an even higher activation energy for recrystallization, 2.44 eV, in very good agreement with the value measured in the experiments, 2.7 eV.[67] IV pairs that lie on the planar $a/c$ interface are surrounded by more IV pairs than those on the amorphous sphere. In the limit, as we have

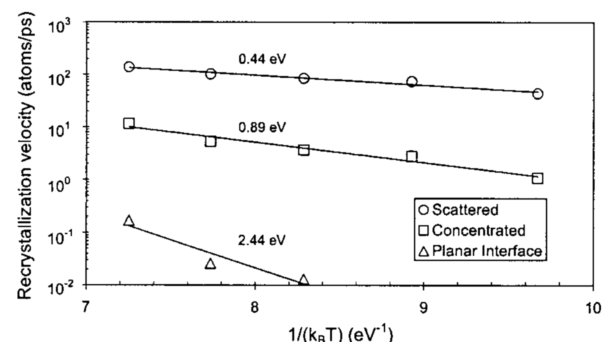


FIG. 27. Arrhenius plot of the recrystallization velocity in samples with scattered and concentrated damage. The recrystallization velocity of a planar $a/c$ interface is also shown. Lines are best fits to each data set. Activation energies are represented besides the corresponding line.

Downloaded 28 Oct 2008 to 192.84.153.250. Redistribution subject to AIP license or copyright; see http://jap.aip.org/jap/copyright.jsp

shown, a pure amorphous matrix would be described by a IV pair completely surrounded by other IV pairs. The recombination of such a IV pair, equivalent to the generation of a crystal embryo in the amorphous phase, cannot be studied by MD techniques because it would imply prohibitively long simulation times. However, the activation energy for crystal nucleation in a pure *a*-Si matrix has been experimentally determined to be 5 eV.[83] Therefore, the higher the number of surrounding IV pairs, the higher the activation energy for IV pair recombination. These energies range from 0.43 eV for an isolated IV pair to 5 eV for a fully coordinated IV pair.

These results may help to get some insight on the long-standing discussion whether irradiation-induced amorphization in Si takes place homogeneously or heterogeneously. Lewis and Nieminen proposed a microscopic model of Si amorphization using MD techniques.[213] From their simulations they conclude that amorphization can only take place heterogeneously, from defect clusters surrounded by damaged crystal. They observed as well that uniform distributions of point defects did not produce amorphization. However, our results suggest that homogeneous amorphization can take place by uniform accumulation of IV pairs when a critical concentration (which depends on temperature) is reached. These results may explain why it is possible to achieve Si amorphization by light ions such as B, or even with electron irradiation at very low temperatures.[167] Electrons are very light particles which presumably create isolated IV pairs and point defects. As we have proved, the IV pair lifetime is very short at room temperature, but at cryogenic temperatures they could survive and accumulate as the electron irradiation dose increases. When the IV pair concentration reaches the critical value (around 25%), the lattice collapses spontaneously to the amorphous state (homogeneous amorphization). The critical concentration can also be reached locally in the amorphous pockets produced when irradiating Si with heavy ions,[125] such as As. During the collisional phase, the ion produces highly damaged zones which, as previously mentioned, are similar to regions with high concentration of IV pairs. These amorphous zones, or a part of them, have longer lifetimes and thus can survive between successive cascades and act as nuclei for damage accumulation (heterogeneous amorphization). The amorphization process is favored if the surrounding crystal lattice is already distorted by the presence of point defects.[213]

## B. Kinetic Monte Carlo simulations

MD simulations provide the physical insight into the amorphization process at atomic level. However, this method is limited by the system sizes ($<10^6$ atoms) and simulation times ($<1$ ns) that can be treated. In the nonlattice kMC simulation technique only lattice defects are considered.[214] Thus, larger system cells and longer simulation times can be handled because the high frequency vibrational movement of the Si lattice atoms is ignored and the simulation concentrates only on relevant defect events (diffusion, emission from clusters, IV pair recombination, etc.) of much lower frequencies. These events and defect interactions have to be explicitly specified by atomic parameters such as diffusion coefficients or binding energies. These parameters are extracted from MD simulations or from experiments.[24] The BCA code MARLOWE (Ref. 120) is used to generate the implantation cascades. The coordinates of generated defects are fed to the kMC simulator at intervals of time determined by the dose rate. During this time, defect diffusion and interaction events occur at a rate that depends on the sample temperature, thus accounting for the dynamic anneal during the implantation process. This scheme is repeated until the specified dose is reached. Afterward, subsequent anneals can be simulated.

### 1. Description of the model

The damage generated in implantation cascades consists of Si self-interstitials, vacancies, and IV pairs. These simple defects can agglomerate and form more complex structures leading to defect clusters and amorphous pockets.[214] IV pairs form when Si self-interstitials and vacancies are within the capture radius of each other,[194] and also directly during the collision cascade.[197] Si self-interstitials or vacancies surrounded by IV pairs are called *amorphous interstitials or amorphous vacancies*, respectively. The rearrangement of these *amorphous defects* during regrowth is simulated by allowing its movement within the amorphous zone. Defects are confined mostly to the amorphous region by imposing a large increase in energy if they move toward the crystalline side. The surface is considered as an efficient sink for Si self-interstitials and vacancies, but it provides a *virtual* layer of IV pairs since it is known to act as a nucleation site for amorphization,[155] and also because when an amorphous layer extends to the surface the regrowth does not advance from there.[145]

Based on the previously mentioned MD studies, the IV pair is used as the elementary unit to describe the amorphous material. Each IV pair is locally characterized by the number of neighboring IV pairs. Its recombination rate decreases as the number of neighboring IV pair increases. We assign an activation energy of 0.43 eV to the isolated IV pair (0 neighbors). The experimentally measured activation energy for recrystallization of a planar $a/c$ interface, 2.7 eV,[67] provides us with another parameter to characterize the recombination rate of IV pairs with about half of the total coordination number. IV pairs embedded into an amorphous matrix (completely surrounded by neighboring IV pairs, and thus with full coordination) have an activation energy of 5 eV.[83] Intermediate coordination numbers have interpolated activation energies.[212]

### 2. Morphology and annealing behavior of amorphous regions

The local characterization of the disordered atoms allows the model to capture any damage morphology that may arise from irradiation cascades, as well as the characteristic regrowth behavior observed in the experiments. This can be seen in the schematic of Fig. 28. In the model, the continuous amorphous layer is just a particular case of an amorphous pocket. This naturally accounts for similar regrowth properties of amorphous pockets and continuous amorphous

Downloaded 28 Oct 2008 to 192.84.153.250. Redistribution subject to AIP license or copyright; see http://jap.aip.org/jap/copyright.jsp

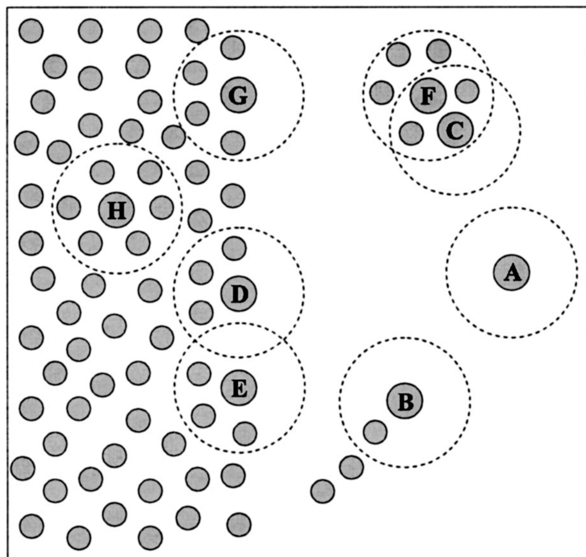


FIG. 28. Scheme of the damage morphology. Each gray circle represents a IV pair, and the dashed lines their interaction radius. Isolated IV pairs (*A*) annihilate first as they do not have any IV neighbor. The amorphous pockets start recombining by the outer IV pairs (*B* and *C*) as the inner ones (*F* or *H*) have more IV neighbors. IV pairs in the interface of elongated pockets (*B*) recombine before than IV pairs in rounded pockets (*C*) as they are surrounded by less IV neighbors. When a IV pair in a planar structure recombines (IV pair missing between *D* and *E*) the whole layer regrows as the surrounding defects (*D* or *E*) have less IV neighbors than the other defects in the layer (*G*).

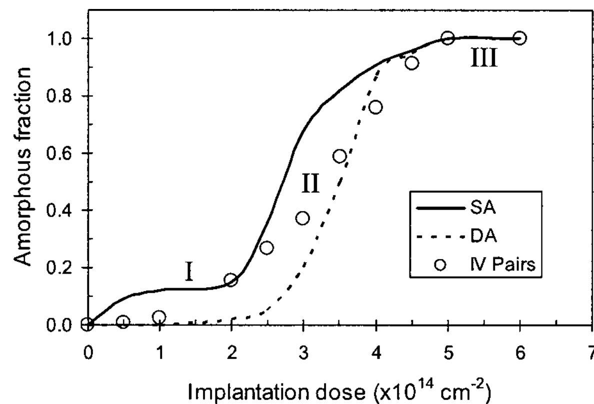


FIG. 29. Dose dependence of the damage produced by 100 keV Si ions at room temperature. Solid and dashed lines correspond to the single-alignment (SA) and double-alignment (DA) Rutherford backscattering spectra from experiments of Ref. 165, respectively. Symbols represent our simulation results.

layers observed experimentally.[135] The regrowth of amorphous regions starts by the IV pairs placed in interfaces with *c*-Si because they have smaller number of IV neighbors than the inner defects. Each amorphous region regrows at a rate that depends on the local coordination of defects. Finite-size amorphous pockets (convex in several sides) naturally regrow at lower temperatures because IV pairs at the interface have less neighbors than they would have in a planar interface. Differences in the annealing times observed for similar amorphous pocket sizes[140] are captured by the variations in recombination rates (determined by the local IV pair coordination) within different geometries.

The steplike behavior of the amorphous pocket recrystallization (see Fig. 8) is easily explained within this model. Plateaus correspond to pockets in which IV pairs lying on the $a/c$ interface have the same coordination. The pockets remain stable until one of these IV pairs recombines, leaving a "hole" (crystalline zone) at the $a/c$ interface. The surrounding IV pairs are left with one less neighbor and therefore they recombine faster. The first IV pair recombination acts thus as a "triggering event" for the recombination of the surrounding IV pairs, producing the steep decreases in the pocket sizes. The regrowth of the planar $a/c$ interface occurs in a similar fashion: a layer-by-layer regrowth occurs activated by the recombination of the first IV pair in each layer.

### 3. Kinetics of damage accumulation

This simple model based on the IV pair quantitatively captures the kinetic features related to the ion-induced amorphization in Si. It encompasses and unifies homogeneous and heterogeneous mechanisms. The nucleation of the amorphous phase consists in the formation of IV pair structures with enough number of IV neighbors to be stable. At the appropriate temperatures, these amorphous embryos can be either small IV pair complexes generated in dilute cascades (homogeneous nucleation) or dense IV pair agglomerates formed in the cascades of heavy ions (heterogeneous amorphization). When there is significant dynamic anneal, preexisting amorphous pockets or planar $a/c$ interfaces can act as nucleation sites.[56,164] Isolated IV pairs may not be able to survive by themselves but if they interact with a preexisting amorphous region, the generated IV pairs will have more IV neighbors and become stable. IV pairs are thus added to the amorphous zone producing its growth.

The cooperative nature of the amorphization phenomena, which is manifested in the superlinear behavior of the accumulated damage versus dose, is a consequence of the increased stability of the IV pairs with the number of IV neighbors. Figure 29 shows the experimental[165] and simulated results on this matter for a 100 keV Si implant at room temperature. For low doses the amorphous fraction grows slowly, until a sharp increase occurs near a given (transition) dose. This happens because the damage is dilute for low doses, so only a small percentage of the generated damage survives (region I). As the dose increases and the damage reaches certain level, IV pairs start interacting and become more stable. Therefore, a larger percentage of the generated damage survives, resulting in its superlinear increase with dose (region II). The process of adding more damage saturates when amorphization is reached and new cascades just move atoms already displaced from their lattice positions (region III).

One of the most complex phenomena to model is the critical equilibrium that occurs between amorphization and recrystallization processes in Si as the lattice tends to recover from damage generated during ion-beam irradiation. The implant dose rate (time between successive cascades) and substrate temperature determine the probability of the damage from each cascade surviving until the arrival of a new cascade, and thus the rate of damage accumulation. The effect of the dose rate and temperature for 1 MeV Si implants is

Downloaded 28 Oct 2008 to 192.84.153.250. Redistribution subject to AIP license or copyright; see http://jap.aip.org/jap/copyright.jsp

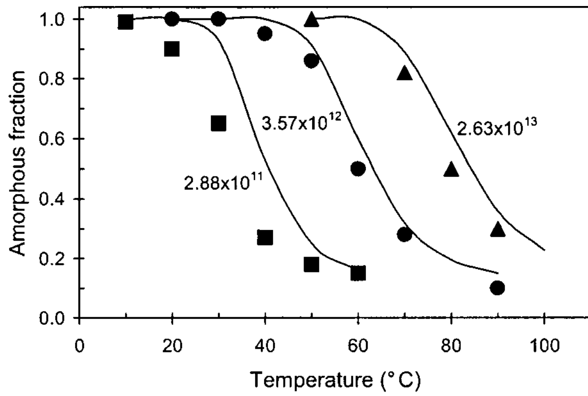


FIG. 30. Amorphous fraction vs substrate temperature for 1 MeV Si implants to a dose of $10^{15}$ cm$^{-2}$ with several dose rates (in cm$^{-2}$ s$^{-1}$). Solid symbols correspond to the experimental data of Ref. 100, obtained from Rutherford backscattering spectra. Solid lines represent our simulation results.

represented in Fig. 30. As can be seen, in the case of Si implants the critical temperature for amorphization, $T_C$, lies around room temperature.[100] The amorphous fraction (IV pair concentration relative to the atomic Si density) can be parametrized with a simple reverse exponential

$$\text{Amorphous fraction} = a + b\frac{1}{1+\exp[c(T-T_C)]}, \tag{9}$$

where $c$ describes the width of the phase transition, and $a$ and $a+b$ set the limits for $T \gg T_C$ and $T \ll T_C$, respectively. In Fig. 31 the critical temperatures for amorphization versus ion flux for Si and Ge implants resulting from our simulations are plotted and compared with experiments.[169]

The average lifetime of a given IV pair in an amorphous zone is given by

$$t_a = t_o \exp(E_a/k_B T), \tag{10}$$

where $t_o$ is the prefactor, $E_a$ the activation energy for recombination, $k_B$ the Boltzmann constant, and $T$ the temperature. The critical temperature for a given dose rate corresponds to that at which $t_a \sim t_s$, being $t_s$ the time for arrival of two successive ions to the same region. Because of the exponential temperature dependence, small changes in $T$ induce large

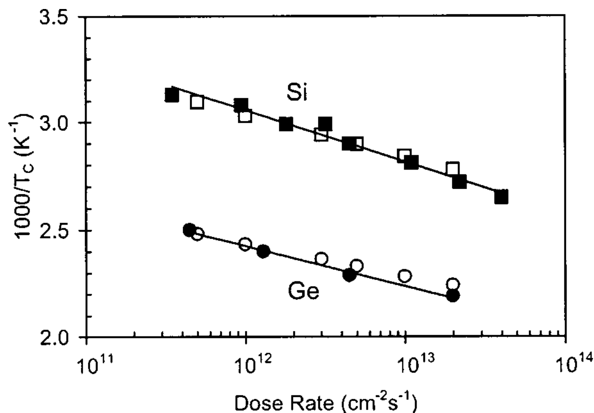


FIG. 31. Critical temperature as a function of ion dose rate for 80 keV Si and Ge implants to a dose of $10^{15}$ cm$^{-2}$. Open symbols correspond to simulation results. Solid symbols are from the experiments of Ref. 169.

variations in $t_a$ and, therefore, in the probability of the defect surviving during $t_s$. An increase in the dose rate (reduction in $t_s$) shifts the temperature at which $t_s \sim t_a$ toward higher values.

Implantation cascades produce a great variety of damage configurations, and basically the whole spectrum of activation energies from 0.4 eV to 5 eV are present. For the damage to accumulate and produce a continuous amorphous layer, a fraction of the generated damage in each cascade has to survive. At low $T$ most defects follow $E_a \gg k_B T \ln(t_s/t_o)$ and survive. At high $T$, all defects recombine. In those extreme cases there is no temperature dependence. However, in the regime where damage generation closely balances damage annihilation, several activation energies were measured for the onset of amorphization for different ions,[169] which in principle were associated to different defects. In our model, the structural defect that causes amorphization is the same for all ions, but it has different energy barriers for recombination as a function of the surrounding neighborhood. Light ions produce mostly isolated or small IV pair complexes. Therefore, small values of $E_a$ are governing the critical equilibrium that allows the onset of amorphization. On the contrary, heavier ions produce a larger fraction of denser damage structures with larger $E_a$ values. This also explains why the critical temperature for amorphization $T_C$ is higher for heavier ions.

#### *4. Residual damage after regrowth*

For the fundamental understanding of the amorphization process, experiments are generally carried out near the critical regime where significant anneal takes place during the implantation process. However, from a more applied point of view, implant parameters are chosen either to clearly prevent amorphization or to produce a sufficiently thick amorphous layer. A low thermal budget (a few minutes at 550 °C) is enough to regrow the amorphous regions. The nature and distribution of residual damage after this annealing is very different depending on whether the implant produces a continuous amorphous layer or just small amorphous regions. This model treats amorphizing and nonamorphizing implants in a consistent way, and the annealing behavior is determined by the morphology of the damage. The IV pair defect contains no excess or deficit of atoms, so when it annihilates there are no net point defects released in the lattice. However, extended amorphous regions frequently contain an excess or deficit of atoms compared to the perfect crystal.[122,215] These unbalanced atoms are moved along the regrowing interfaces. When the amorphous regions completely regrow these atoms are left behind as ordinary Si self-interstitials or vacancies.[122]

In Fig. 32 we show three snapshots of the damage evolution of a 5 keV Si implant to a dose of $10^{14}$ cm$^{-2}$. This implantation produces significant amount of damage but not a continuous amorphous layer. During the subsequent annealing amorphous pockets regrow quickly and, since they are disconnected, the local excess of Si self-interstitials and vacancies is left behind. The implanted ion generally sits in a substitutional position and, consequently, one Si self-interstitial per implanted ion is generated in excess over the

Downloaded 28 Oct 2008 to 192.84.153.250. Redistribution subject to AIP license or copyright; see http://jap.aip.org/jap/copyright.jsp

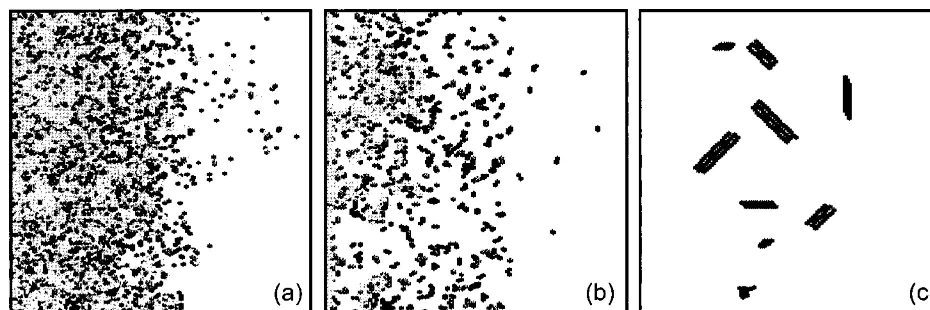


FIG. 32. Damage evolution of a 5 keV Si implant to a dose of $10^{14}$ cm$^{-2}$. Black and dark gray points represent Si self-interstitials and vacancies, respectively. Light gray points correspond to IV pairs. (a) Damage after implantation at room temperature. (b) Damage during the temperature ramp. (c) Defects resulting after annealing at 800 °C.

number of vacancies. Therefore, even though local excesses of both kinds of defects may appear momentarily, these tend to recombine (after forming first a metastable IV pair). Only the one Si self-interstitial per implanted ion that has no vacancy partner survives for longer time. These interstitials agglomerate into extended defects until they finally dissolve driving TED of interstitial diffuser atoms.[13,24,216] Since only the net excess of defects remains after the rapid regrowth of disconnected amorphous pockets, the +1 *model*[216] and all the well-established results for subamorphizing implants and defect evolution[13,217] are valid within this model.

In Fig. 33 snapshots for a 5 keV Si implant to a dose of $10^{15}$cm$^{-2}$ are shown. After the implant, a continuous amorphous layer is formed. During annealing, amorphous pockets beyond the $a/c$ interface quickly regrow and excess Si self-interstitials and vacancies in that region remain. The excess or deficit atoms contained within the amorphous layer are swept out as the interface regrows layer by layer. When the amorphous layer extends from the surface into the bulk of the crystal, as in this case, unbalanced atoms are incorporated at the surface, leaving the regrown amorphous layer free of defects.[145] The remaining defects beyond the $a/c$ interface agglomerate into more complex structures, such as {113} defects or loops, whose dissolution requires higher thermal budgets. When the amorphous layer is buried, the excess defects swept along by the two simultaneously advancing $a/c$ interfaces cannot be absorbed by a free surface, and thus a shell of defects appears along the plane where the two interfaces merge.[143]

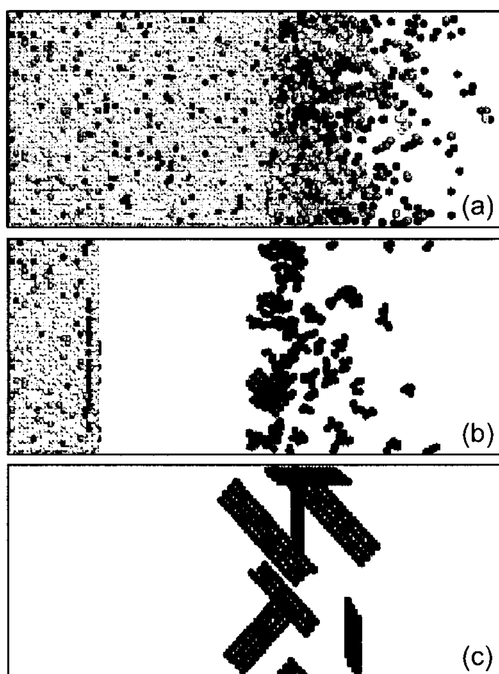


FIG. 33. Damage evolution of a 5 keV Si implant to a dose of $10^{15}$ cm$^{-2}$. Black and dark gray points represent Si self-interstitials and vacancies, respectively. Light gray points correspond to IV pairs. (a) Damage after implantation at room temperature. (b) The damage annealing at 550 °C shows the planar regrowth of the continuous amorphous layer. Defects within this layer are swept out as the regrowth takes place. Defects beyond the original $a/c$ interface remains. (c) Defects resulting after annealing at 800 °C.

In Fig. 34 we compare the residual damage resulting from Si implants at doses of $10^{14}$, $10^{15}$, and $2\times10^{15}$ cm$^{-2}$ after a short anneal of 550 °C for 200 s, enough to regrow the thicker amorphous regions formed. For a subamorphizing implant ($10^{14}$ cm$^{-2}$), the residual damage consists of a Si interstitial profile that mirrors that of the implanted ion (+1 model). The higher dose implants ($10^{15}$ and $2\times10^{15}$ cm$^{-2}$) form a continuous amorphous layer which is deeper as the dose increases. Even though the dose changes by a factor of 2, the amount of residual damage beyond the $a/c$ interface is similar in both amorphizing implants.

The control of the exact position of the planar $a/c$ interface is important for the fabrication of Si devices. Because

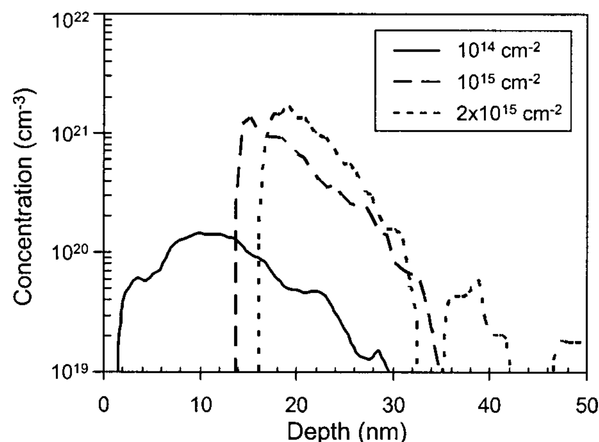


FIG. 34. Residual damage profile after a 200 s anneal at 550 °C for 5 keV Si implants to doses of $10^{14}$, $10^{15}$, and $2\times10^{15}$ cm$^{-2}$. All implants are carried out with a dose rate of $2\times10^{12}$cm$^{-2}$s$^{-1}$ and at a substrate temperature of 20 °C.

Downloaded 28 Oct 2008 to 192.84.153.250. Redistribution subject to AIP license or copyright; see http://jap.aip.org/jap/copyright.jsp

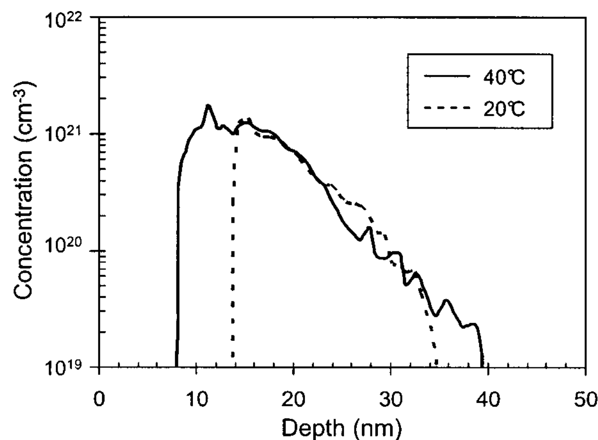


FIG. 35. Residual damage profile after a 200 s anneal at 550 °C for 5 keV Si implants at substrate temperature of 20 and 40 °C. Both implants were carried out to a dose of $10^{15}$ cm$^{-2}$ with a dose rate of $2\times10^{12}$ cm$^{-2}$ s$^{-1}$.

the melting temperature of *a*-Si is slightly lower than that of *c*-Si, preamorphization prior to LTA processes is frequently used to have a better control of the melted depth.[33] The position of the *a*/*c* interface also determines the amount of residual damage beyond it, and this has important consequences on dopant diffusion and activation.[35] For a given ion, implant energy and dose are generally the most relevant parameters for determining the position and thickness of the amorphous layer, but variations in the implant temperature or dose rate can also affect the exact position of the *a*/*c* interface.

As we have seen in Sec. IV, the kinetics of amorphization is governed by the rate of damage accumulation that results from the balance between damage generation and its dynamical anneal. Any factor that increases the dynamic anneal (for instance, higher temperatures or lower dose rates) causes the annihilation of a larger fraction of generated defects and, consequently, a reduction in the thickness of the amorphous layer. This effect is shown in Fig. 35 for implant temperatures of 20 and 40 °C. This slight temperature increase could arise from self-heating during the implantation process. Although the *a*/*c* interface is only a few nanometers shallower, the amount of residual damage is significantly higher for the implant at 40 °C. This example reveals the importance of a careful control of all implant parameters.

## VII. CONCLUSIONS

In this paper we have reviewed experimental results and theoretical models concerning ion-beam-induced amorphization and SPEG in Si. These phenomena have been known from the early 1970s, and since then they have been the subject of a great number of studies. There is now a renewed interest because of their technological relevance for the semiconductor industry. For example, high implant doses of As or $BF_2$ required to achieve high levels of carrier concentration induce amorphization of the Si lattice. In the case of B implantation, preamorphizing Ge implants followed by SPEG are carried out as a way of obtaining high electrical activation with reduced thermal budgets.[12]

Energetic implanted ions generate different damage structures, ranging from isolated point defects and defect clusters to the direct formation of amorphous regions. The annealing behavior of amorphous pockets is not associated to a unique activation energy. Rather than a smooth exponential decay, plateaus and step regions are observed. Also, their stability is not only determined by their size (total number of disordered atoms) but also by their morphology. These anomalous features have hampered their experimental and theoretical characterization. A large number of experiments have evidenced other intriguing features in the kinetics of amorphization, such as the superlinear dependence of the accumulated damage versus dose, the super additivity of the damage with the number of simultaneously implanted atoms or the critical nature of the *c*-*a* transition under conditions where the dynamic annealing rate closely balances the damage production rate.

Under traditional models, amorphization was considered to be the result of the accumulation of simple defects (homogeneous models) or the overlap of locally amorphous regions (heterogeneous models). Among the different defect structures suggested to account for the observed structural and kinetic characteristics of the amorphous phase, we have shown that the atomistic model based on the IV pair is able to explain and quantitatively reproduce the experimental observations. Within this model, amorphous layers are a particular case of amorphous pockets, which are considered to be an agglomerate of IV pairs. The key feature of the model is the local characterization of the activation energy for recrystallization of each IV pair as a function of the number of neighboring IV pairs. This accounts for the observed differences in the annealing behavior of various damage structures and for the singular features of the amorphization and recrystallization kinetics in Si. This model unifies homogeneous and heterogeneous descriptions of the amorphous phase nucleation. Although it has been developed for Si, it could be extended to other materials with the appropriate parameters. As has been pointed out, it is very difficult to experimentally observe the IV defect. Full validation of the model will occur when the IV defects are experimentally characterized.

We have shown that the position of the *a*/*c* interface, and so, the residual damage, can be altered by small changes in the implant temperature, fluence, and flux. The amount and stability of this residual damage strongly influence dopant diffusion and activation.[31] Detailed models for amorphization and regrowth that take into account all implant parameters are thus required for process simulators with predictive capabilities.

Further modeling efforts are required to account for the role of impurities in *a*-Si. The effect of impurities in the regrowth velocity can be easily taken into account by considering an activation energy dependent on the impurity concentration. More complicated effects, such as diffusion, segregation, and precipitation in *a*-Si, will require further research on the detailed interactions between impurities and defects in the amorphous phase.[218–221] These phenomena are important since they could play a significant role when introducing the high dopant concentrations needed for the fabrication of future Si devices.[222–225]

Downloaded 28 Oct 2008 to 192.84.153.250. Redistribution subject to AIP license or copyright; see http://jap.aip.org/jap/copyright.jsp

## ACKNOWLEDGMENTS

The authors would like to express their gratitude to George H. Gilmer for many stimulating discussions and to John M. Poate for encouraging them to write this paper. This work was supported by the Spanish DGICYT under Project No. BFM 2001-2250 and the JCYL Consejería de Educación y Cultura under Project No. VA-010/02.

[1]J. Bloch, J. Nucl. Mater. **6**, 203 (1962).
[2]D. E. Luzzi and M. Meshii, Res. Mech. **21**, 207 (1987).
[3]W. J. Meng, P. R. Okamoto, L. J. Thompson, L. J. Kestel, and L. E. Rehn, Appl. Phys. Lett. **53**, 1820 (1988).
[4]S. K. Bahl and S. M. Bhagat, J. Non-Cryst. Solids **17**, 409 (1975).
[5]K. Minowa and K. Sumino, Phys. Rev. Lett. **69**, 320 (1992).
[6]D. R. Clarke, M. C. Kroll, P. D. Kirchner, R. F. Cook, and B. J. Hockey, Phys. Rev. Lett. **60**, 2156 (1988).
[7]A. G. Cullis, H. C. Webber, N. G. Chew, J. M. Poate, and P. Baeri, Phys. Rev. Lett. **49**, 219 (1982).
[8]E. Chason, *et al.*, J. Appl. Phys. **81**, 6513 (1997).
[9]L. Csepregi, E. F. Kennedy, J. W. Mayer, and T. W. Sigmon, J. Appl. Phys. **49**, 3906 (1978).
[10]M. Y. Tsai and B. G. Streetman, J. Appl. Phys. **50**, 183 (1979).
[11]J. Narayan, O. W. Holland, and B. R. Appleton, J. Vac. Sci. Technol. B **1**, 871 (1983).
[12]E. Landi, A. Armigliato, S. Solmi, R. Köghler, and E. Wieser, Appl. Phys. A: Mater. Sci. Process. **A47**, 359 (1998).
[13]P. A. Stolk *et al.*, J. Appl. Phys. **81**, 6031 (1997).
[14]S. Solmi, F. Baruffaldi, and R. Canteri, J. Appl. Phys. **69**, 2135 (1991).
[15]D. J. Eaglesham, P. A. Stolk, H.-J. Gossmann, and J. M. Poate, Appl. Phys. Lett. **65**, 2305 (1994).
[16]N. E. B. Cowern *et al.*, Phys. Rev. Lett. **82**, 4460 (1999).
[17]R. Raman, M. E. Law, V. Krishnamoorthy, K. S. Jones, and S. B. Herner, Appl. Phys. Lett. **74**, 1591 (1999).
[18]A. Claverie, B. Colombeau, G. B. Assayag, C. Bonafos, F. Cristiano, M. Omri, and B. de Mauduit, Mater. Sci. Semicond. Process. **3**, 269 (2000).
[19]F. Cristiano, J. Grisolia, B. Colombeau, M. Omri, B. de Mauduit, A. Claverie, and F. L. Giles, J. Appl. Phys. **87**, 8420 (2000).
[20]S. Libertino, S. Coffa, and J. L. Benton, Phys. Rev. B **63**, 195206 (2001).
[21]M. E. Law, K. S. Jones, S. K. Earles, A. D. Lilak, and J.-W. Xu, in *Materials Modification and Synthesis by Ion Beam Processing Symposium*, edited by D. E. Alexander, N. W. Cheung, B. Park, and W. Skorupa (Materials Research Society, Pittsburgh, 1997).
[22]E. Lampin, F. Cristiano, Y. Lamrani, A. Claverie, B. Colombeau, and N. E. B. Cowern, J. Appl. Phys. **94**, 7520 (2003).
[23]I. Avci, M. E. Law, E. Kuryliw, A. F. Saavedra, and K. S. Jones, J. Appl. Phys. **95**, 2452 (2004).
[24]L. Pelaz, M. Jaraiz, G. H. Gilmer, H.-J. Gossmann, C. S. Rafferty, D. J. Eaglesham, and J. M. Poate, Appl. Phys. Lett. **70**, 2285 (1997).
[25]M.-J. Caturla, T. D. de la Rubia, and M. D. Johnson, Appl. Phys. Lett. **72**, 2736 (1998).
[26]L. Pelaz, G. H. Gilmer, H.-J. Gossmann, C. S. Rafferty, M. Jaraiz, and J. Barbolla, Appl. Phys. Lett. **74**, 3657 (1999).
[27]L. S. Robertson, M. E. Law, K. S. Jones, L. M. Rubin, J. Jackson, P. Chi, and D. S. Simons, Appl. Phys. Lett. **75**, 3844 (1999).
[28]W. Windl, M. M. Bunea, R. Stumpf, S. T. Dunham, and M. P. Masquelier, Phys. Rev. Lett. **83**, 4345 (1999).
[29]T. J. Lenosky, B. Sadigh, S. K. Theiss, M.-J. Caturla, and T. D. de la Rubia, Appl. Phys. Lett. **77**, 1834 (2000).
[30]A. D. Lilak, M. E. Law, L. Radic, K. S. Jones, and M. Clark, Appl. Phys. Lett. **81**, 2244 (2002).
[31]M. Aboy, L. Pelaz, L. A. Marqués, J. Barbolla, A. Mokhberi, Y. Takamura, P. B. Griffin, and J. D. Plummer, Appl. Phys. Lett. **83**, 4166 (2003).
[32]R. Lindsay *et al.*, in *CMOS Front-End Materials and Process Technology*, edited by T.-J. King, B. Yu, R.J.P. Lander, and S. Saito, Mater. Res. Soc. Symp. Proc. 765, D7.4.1 (Materials Research Society, Pittsburgh, 2003).
[33]Y. Takamura, S. H. Jain, P. B. Griffin, and J. D. Plummer, J. Appl. Phys. **92**, 230 (2002).
[34]J.-Y. Jin, J. Liu, U. Jeong, S. Mehta, and K. Jones, J. Vac. Sci. Technol. B **20**, 422 (2002).
[35]B. J. Pawlak *et al.*, Appl. Phys. Lett. **84**, 2055 (2004).
[36]See *International technology roadmap for semiconductors*, http://public.itrs.net/
[37]H. Cerva and G. Hobler, J. Electrochem. Soc. **139**, 3631 (1992).
[38]G. Hobler and G. Otto, Mater. Sci. Semicond. Process. **6**, 1 (2003).
[39]S. Roorda, W. C. Sinke, J. M. Poate, D. C. Jacobson, S. Dierker, B. S. Dennis, D. J. Eaglesham, F. Spaepen, and P. Fuoss, Phys. Rev. B **44**, 3702 (1991).
[40]S. C. Moss and J. F. Graczyk, Phys. Rev. Lett. **23**, 1167 (1969).
[41]M. H. Brodsky, R. Title, K. Weiser, and G. D. Pettit, Phys. Rev. B **1**, 2632 (1970).
[42]M. H. Brodsky, D. Kaplan, and J. F. Ziegler, Appl. Phys. Lett. **21**, 305 (1972).
[43]J. S. Custer, M. O. Thompson, D. C. Jacobson, J. M. Poate, S. Roorda, W. C. Sinke, and F. Spaepen, Appl. Phys. Lett. **64**, 437 (1994).
[44]P. A. Stolk, F. W. Saris, A. J. M. Berntsen, W. V. der Weg, L. T. Sealy, R. C. Barklie, G. Krötz, and G. Müller, J. Appl. Phys. **75**, 7266 (1994).
[45]D. E. Polk and D. S. Boudreaux, Phys. Rev. Lett. **31**, 92 (1973).
[46]F. Wooten, K. Winer, and D. Weaire, Phys. Rev. Lett. **54**, 1392 (1985).
[47]F. Wooten and D. Weaire, Solid State Phys. **40**, 1 (1987).
[48]S. Roorda, J. M. Poate, D. C. Jacobson, B. S. Dennis, S. Dierker, and W. C. Sinke, Appl. Phys. Lett. **56**, 2097 (1990).
[49]S. Coffa, F. Priolo, and A. Battaglia, Phys. Rev. Lett. **70**, 3756 (1993).
[50]I.-H. Lee and K. J. Chang, Phys. Rev. B **50**, 18083 (1994).
[51]W. G. Spitzer, G. K. Hubler, and T. Kennedy, Nucl. Instrum. Methods Phys. Res. **209–210**, 309 (1983).
[52]S. T. Pantelides, Phys. Rev. Lett. **57**, 2979 (1986).
[53]G. N. van den Hoven, Z. N. Liang, L. Niesen, and J. S. Custer, Phys. Rev. Lett. **68**, 3714 (1992).
[54]R. Tsu, J. G. Hernandez, and F. H. Pollak, Solid State Commun. **54**, 447 (1985).
[55]W. C. Sinke, T. Warabisako, M. Miyao, T. Tokuyama, S. Roorda, and F. W. Saris, J. Non-Cryst. Solids **99**, 308 (1988).
[56]A. Battaglia and S. U. Campisano, J. Appl. Phys. **74**, 6058 (1993).
[57]E. P. Donovan, G. K. Hubler, and C. N. Wadell, Nucl. Instrum. Methods Phys. Res. B **19**, 590 (1987).
[58]J. E. Fredrickson, C. N. Waddell, W. G. Spitzer, and G. K. Hubler, Appl. Phys. Lett. **40**, 172 (1982).
[59]P. A. Thomas, H. M. Brodsky, D. Kaplan, and D. Lepine, Phys. Rev. B **18**, 3059 (1978).
[60]S. Roorda, S. Doorn, W. C. Sinke, P. M. L. O. Scholte, and E. van Loenen, Phys. Rev. Lett. **62**, 1880 (1989).
[61]E. P. Donovan, F. Spaepen, J. Poate, and D. Jacobson, Appl. Phys. Lett. **55**, 1516 (1989).
[62]S. Coffa, J. M. Poate, W. Frank, and W. Gustin, Phys. Rev. B **45**, 8355 (1992).
[63]C. A. Volkert, J. Appl. Phys. **74**, 7107 (1993).
[64]K. W. Wang, W. G. Spitzer, G. K. Hubber, and D. K. Sadana, J. Appl. Phys. **58**, 4553 (1985).
[65]J. W. Mayer, L. Eriksson, S. T. Picraux, and J. A. Davis, Can. J. Phys. **46**, 663 (1968).
[66]L. Csepregi, J. W. Mayer, and T. W. Sigmon, Phys. Lett. **54**, 157 (1975).
[67]G. L. Olson and J. A. Roth, Mater. Sci. Rep. **3**, 1 (1988).
[68]N. Nagasima and N. Kubota, J. Vac. Sci. Technol. **1**, 54 (1977).
[69]J. Fan and H. Andersen, J. Appl. Phys. **52**, 4003 (1981).
[70]L. Csepregi, E. F. Kennedy, T. J. Gallagher, J. W. Mayer, and T. W. Sigmon, J. Appl. Phys. **48**, 4234 (1977).
[71]S. A. Kokorowski, G. L. Olsen, and L. D. Hess, J. Appl. Phys. **53**, 921 (1982).
[72]A. Lietoila, A. Wakita, T. W. Sigmon, and J. Gibbons, J. Appl. Phys. **53**, 4399 (1982).
[73]E. P. Donovan, F. Spaepen, D. Turnbull, J. M. Poate, and D. C. Jacobson, J. Appl. Phys. **57**, 1795 (1985).
[74]J. S. Williams, *Surface Modification and Alloying* (Plenum, New York, 1983).
[75]I. Suni, G. Goltz, M. G. Grimaldi, M.-A. Nicolet, and S. S. Lau, Appl. Phys. Lett. **40**, 269 (1982).
[76]J. S. Williams and R. G. Elliman, Phys. Rev. Lett. **51**, 1069 (1983).
[77]E. F. Kennedy, L. Csepregi, J. W. Mayer, and T. W. Sigmon, J. Appl. Phys. **48**, 4241 (1977).
[78]M. Wittmer, J. Roth, P. Revesz, and J. W. Mayer, J. Appl. Phys. **49**, 5207 (1978).
[79]K. F. Kelton, A. L. Greer, and C. V. Thompson, J. Chem. Phys. **79**, 6261 (1983).
[80]C. Spinella, S. Lombardo, and F. Priolo, J. Appl. Phys. **84**, 5383 (1998).
[81]K. Zellama, P. Germain, S. Squelard, J. C. Bourgoin, and P. A. Thomas, J. Appl. Phys. **50**, 6995 (1979).

**Downloaded 28 Oct 2008 to 192.84.153.250. Redistribution subject to AIP license or copyright; see http://jap.aip.org/jap/copyright.jsp**

[82] R. B. Iverson and R. Reif, J. Appl. Phys. **62**, 1675 (1987).
[83] Y. Masaki, P. G. LeComber, and A. G. Fitzgerald, J. Appl. Phys. **74**, 129 (1993).
[84] E. P. Donovan, F. Spaepen, D. Turnbull, J. M. Poate, and D. C. Jacobson, Appl. Phys. Lett. **42**, 698 (1983).
[85] M. O. Thompson, G. J. Galvin, J. W. Mayer, P. S. Peercy, J. M. Poate, D. C. Jacobson, A. G. Cullis, and N. G. Chew, Phys. Rev. Lett. **52**, 2360 (1984).
[86] P. Baeri, G. Foti, J. M. Poate, and A. G. Cullis, Phys. Rev. Lett. **45**, 2036 (1980).
[87] S. R. Elliot, *Physics of Amorphous Materials* (Wiley, New York, 1990).
[88] A. G. Cullis, H. C. Webber, and N. G. Chew, Appl. Phys. Lett. **40**, 998 (1982).
[89] D. Turnbull, in *Beam-solid Interactions and Phase Transformations*, edited by H. Kurz, G. L. Olson, and J. M. Poate, Symposia Proceedings No. 51 (Materials Research Society (MRS), Pittsburgh, 1986), p. 71.
[90] J. F. Gibbons, Proc. IEEE **60**, 1062 (1972).
[91] M. Ishimaru, S. Harada, and T. Motooka, J. Appl. Phys. **81**, 1126 (1997).
[92] J. Yamasaki, S. Takeda, and K. Tsuda, Phys. Rev. B **65**, 115213 (2002).
[93] G. Bai and M. A. Nicolet, J. Appl. Phys. **70**, 649 (1991).
[94] Y. Waseda and K. Suzuki, Z. Phys. B **20**, 339 (1975).
[95] J. M. Haile, *Molecular Dynamics Simulations: Elementary Methods* (Wiley, New York, 1992).
[96] K. Laaziri, S. Kycia, S. Roorda, H. Chicoine, J. L. Robertson, J. Wang, and C. S. Moss, Phys. Rev. Lett. **82**, 3460 (1999).
[97] I. Stich, R. Car, and M. Parrinello, Phys. Rev. Lett. **63**, 2240 (1989).
[98] F. Priolo and E. Rimini, Mater. Sci. Rep. **5**, 319 (1990).
[99] O. W. Holland, Appl. Phys. Lett. **54**, 320 (1989).
[100] P. J. Schultz, C. Jagadish, M. C. Ridgway, R. G. Elliman, and J. S. Williams, Phys. Rev. B **44**, 9118 (1991).
[101] J. A. Davies, G. Foti, L. M. Howe, J. B. Mitchell, and K. B. Winterbon, Phys. Rev. Lett. **34**, 1441 (1975).
[102] T. Motooka and O. W. Holland, Appl. Phys. Lett. **61**, 3005 (1992).
[103] T. Motooka and O. W. Holland, Appl. Phys. Lett. **58**, 2360 (1991).
[104] T. Motooka, F. Kobayashi, P. Fons, T. Tokuyama, T. Suzuki, and N. Natsuaki, Jpn. J. Appl. Phys., Part 1, **30**, 3617 (1991).
[105] D. Beeman, R. Tsu, and M. F. Thorpe, Phys. Rev. B **32**, 874 (1985).
[106] W. C. Sinke, S. Roorda, and F. W. Saris, J. Mater. Res. **3**, 1202 (1988).
[107] J. R. Dennis and E. B. Hale, J. Appl. Phys. **49**, 1119 (1978).
[108] B. L. Crowder, R. S. Title, M. H. Brodsky, and G. D. Pettit, Appl. Phys. Lett. **16**, 205 (1970).
[109] F. F. Morehead, B. L. Crowder, and R. S. Title, J. Appl. Phys. **43**, 1112 (1972).
[110] H. J. Stein, F. L. Vook, D. K. Brice, J. A. Borders, and S. T. Picraux, in the *Proceedings of First International Conference on Ion Implantation*, edited by L. Chadderton and F. Eisen (Gordon and Breach, New York, 1971), pp. 17–24.
[111] E. C. Baranova, V. M. Gusev, Y. V. Martynenko, C. V. Starinin, and I. B. Haibullin, Radiat. Eff. **18**, 21 (1973).
[112] E. C. Baranova, V. M. Gusev, Y. V. Martynenko, and I. B. Haibullin, Radiat. Eff. **25**, 157 (1975).
[113] T. C. McGill, S. L. Kurtin, and G. A. Schifrin, J. Appl. Phys. **41**, 246 (1970).
[114] J. W. Corbett, *Solid State Physics* (Academic, New York, 1966), Vol. 7.
[115] L. A. Miller, D. K. Brice, A. K. Prinja, and S. T. Picraux, Radiat. Eff. Defects Solids **129**, 127 (1994).
[116] M.-J. Caturla, T. D. de la Rubia, and G. H. Gilmer, in *Materials Synthesis and Processing using Ion beams*, edited by R. J. Culburison, O. W. Holland, K. S. Jones, and K. Maiz, MRS Symposia Proceedings No. 316 (Material Research Society, Pittsburgh, 1994), p. 141.
[117] J. A. Brinkman, J. Appl. Phys. **25**, 961 (1954).
[118] P. Sigmund, Rev. Roum. Phys. **17**, 823 (1972).
[119] J. F. Ziegler, *Stopping and Ranges of Ions in Matter* (Pergamon, New York, 1977).
[120] M. T. Robinson and I. M. Torrens, Phys. Rev. B **9**, 5008 (1974).
[121] K. B. Winterbon, P. Sigmund, and J. B. Sanders, K. Dan. Vidensk. Selsk. Mat. Fys. Medd. **37**, 14 (1970).
[122] T. D. de la Rubia and G. H. Gilmer, Phys. Rev. Lett. **74**, 2507 (1995).
[123] T. D. de la Rubia, R. S. Averback, R. Benedek, and W. E. King, Phys. Rev. Lett. **59**, 1930 (1987).
[124] R. A. Brown, D. Maroudas, and T. Sinno, J. Cryst. Growth **137**, 12 (1994).
[125] M.-J. Caturla, T. D. de la Rubia, L. A. Marqués, and G. H. Gilmer, Phys. Rev. B **54**, 16683 (1996).
[126] L. M. Howe and M. H. Rainville, Nucl. Instrum. Methods Phys. Res. **182**/183, 143 (1981).
[127] L. M. Howe and M. H. Rainville, Nucl. Instrum. Methods Phys. Res. B **19–20**, 61 (1987).
[128] O. W. Holland, M. K. El-Ghor, and C. W. White, Appl. Phys. Lett. **53**, 1283 (1988).
[129] J. W. Corbett, J. Karins, and T. Y. Tan, Nucl. Instrum. Methods Phys. Res. **182–183**, 457 (1981).
[130] W. Jung and H. S. Nwell, Phys. Rev. **132**, 648 (1963).
[131] H. J. Stein, F. L. Vook, and J. A. Borders, Appl. Phys. Lett. **14**, 328 (1969).
[132] A. Claverie, B. Colombeau, F. Cristiano, A. Altibelli, and C. Bonazos, Nucl. Instrum. Methods Phys. Res. B **186**, 281 (2002).
[133] A. P. Knights, F. Malik, and P. G. Colleman, Appl. Phys. Lett. **75**, 466 (1999).
[134] D. A. Thompson, A. Golanski, H. Haugen, L. M. Howe, and J. A. Davies, Radiat. Eff. **50**, 125 (1980).
[135] A. Battaglia, F. Priolo, and E. Rimini, Appl. Phys. Lett. **56**, 2622 (1990).
[136] O. W. Holland, C. W. White, M. K. El-Ghor, and J. D. Budai, J. Appl. Phys. **68**, 2081 (1990).
[137] M. K. El-Ghor, O. W. Holland, C. W. White, and S. J. Pennycook, J. Mater. Res. **5**, 352 (1990).
[138] F. Priolo, A. Battaglia, R. Nicotra, and E. Rimini, Appl. Phys. Lett. **57**, 768 (1990).
[139] R. S. Nelson, *European Conference on Ion Implantation* (Peter Peregrinus, Reading, 1970).
[140] S. E. Donnelly, R. C. Birtcher, V. M. Vishnyakov, and G. Carter, Appl. Phys. Lett. **82**, 1860 (2003).
[141] N. Bernstein, M. J. Aziz, and E. Kaxiras, Phys. Rev. B **61**, 6696 (2000).
[142] D. K. Sadana, M. Strathman, J. Washburn, C. W. Magee, M. Mäenpää, and G. R. Booker, Appl. Phys. Lett. **37**, 615 (1980).
[143] D. K. Sadana, M. Strathman, J. Washburn, and G. R. Booker, J. Appl. Phys. **51**, 5718 (1980).
[144] K. S. Jones, S. Prussin, and E. R. Weber, Appl. Phys. A: Solids Surf. **A45**, 1 (1988).
[145] K. S. Jones, K. Moller, J. Chen, M. Puga-Lambers, B. Freer, J. Berstein, and L. Rubin, J. Appl. Phys. **81**, 6051 (1997).
[146] E. Lampin, V. Senez, and A. Claverie, J. Appl. Phys. **85**, 8137 (1999).
[147] J. Linnros, R. G. Elliman, and W. L. Brown, J. Mater. Res. **3**, 1208 (1988).
[148] R. G. Elliman, J. Linnros, and W. L. Brown, in *Fundamentals of Beam-solid Interactions and Transient Thermal Processing*, edited by Michael J. Aziz, Lynn E. Rehn, and Bernd Stritzker, MRS Symposia Proceedings No. 100 (Materials Research Society, Pittsburgh, 1988), p. 363.
[149] J. Linnros, B. Svensson, and G. Holmen, Phys. Rev. B **30**, 3629 (1984).
[150] J. S. Williams, R. G. Elliman, W. L. Brown, and T. E. Seidel, Phys. Rev. Lett. **55**, 1482 (1985).
[151] J. M. Poate, J. Linnros, F. Priolo, D. C. Jacobson, J. L. Batstone, and M. O. Thompson, Phys. Rev. Lett. **60**, 1322 (1988).
[152] K. A. Jackson, J. Mater. Res. **3**, 1218 (1988).
[153] F. Priolo, C. Spinella, and E. Rimini, Phys. Rev. B **41**, 5235 (1990).
[154] J. S. Custer, A. Battaglia, M. Saggio, and F. Priolo, Phys. Rev. Lett. **69**, 780 (1992).
[155] J. S. Williams, H. H. Tan, R. D. Goldberg, R. A. Brown, and C. Jagadish, in Ref. 116, p. 15.
[156] H. A. Atwater and W. L. Brown, Appl. Phys. Lett. **56**, 30 (1990).
[157] R. D. Goldberg, J. S. Williams, and R. G. Elliman, Phys. Rev. Lett. **82**, 771 (1999).
[158] J. S. Williams, X. Zhu, M. C. Ridgway, M. J. Conway, B. C. Williams, F. Fortuna, M. O. Ruault, and H. Bernas, Appl. Phys. Lett. **77**, 4280 (2000).
[159] A. Battaglia, S. Coffa, F. Priolo, and C. Spinella, Appl. Phys. Lett. **65**, 306 (1994).
[160] J. E. Westmoreland, G. W. Mayer, F. H. Eisen, and B. Welch, Appl. Phys. Lett. **15**, 3088 (1969).
[161] S. T. Picraux, J. E. Westmoreland, J. W. Mayer, R. R. Hart, and O. J. March, Appl. Phys. Lett. **14**, 7 (1969).
[162] S. U. Campisano, S. Coffa, V. Raineri, F. Priolo, and E. Rimini, Nouv. J. Chim. **80–81**, 514 (1993).
[163] F. F. Morehead and B. L. Crowder, Radiat. Eff. **6**, 27 (1970).
[164] R. D. Goldberg, R. G. Elliman, and J. S. Williams, Nucl. Instrum. Methods Phys. Res. B **80/81**, 596 (1993).
[165] O. W. Holland, S. J. Pennycook, and G. L. Albert, Appl. Phys. Lett. **55**, 2503 (1989).
[166] D. N. Seidman, R. S. Averback, P. R. Okamoto, and A. C. Baily, Phys.

Downloaded 28 Oct 2008 to 192.84.153.250. Redistribution subject to AIP license or copyright; see http://jap.aip.org/jap/copyright.jsp

Rev. Lett. **58**, 900 (1987).
[167] S. Takeda and J. Yamasaki, Phys. Rev. Lett. **83**, 320 (1999).
[168] J. R. Dennis and E. B. Hale, Appl. Phys. Lett. **29**, 523 (1976).
[169] R. D. Goldberg, J. S. Williams, and R. G. Elliman, Nucl. Instrum. Methods Phys. Res. B **106**, 242 (1995).
[170] O. W. Holland, D. Fathy, J. Narayan, and O. S. Oen, Radiat. Eff. Defects Solids **90**, 127 (1985).
[171] F. L. Vook, in *Radiation Damage and Defects in Semiconductors*, Inst. Phys. Conf. Ser. No. 16, edited by J. E. Whitehouse (Institute of Physics, London, 1973).
[172] S. Prussin, D. I. Margolese, and R. N. Tauber, J. Appl. Phys. **57**, 180 (1985).
[173] H. J. Stein, Radiat. Eff. **6**, 19 (1970).
[174] S. T. Picraux, W. Weisenberger, and F. L. Vook, Radiat. Eff. **7**, 101 (1971).
[175] S. T. Picraux and F. L. Vook, Radiat. Eff. **11**, 179 (1971).
[176] M. L. Swanson, J. R. Parsons, and C. W. Hoelke, Radiat. Eff. **9**, 249 (1971).
[177] L. T. Chadderton and F. H. Eisen, Radiat. Eff. **7**, 129 (1971).
[178] T. Motooka, Phys. Rev. B **49**, 16367 (1994).
[179] T. Motooka, S. Harada, and M. Ishimaru, Phys. Rev. Lett. **78**, 2980 (1997).
[180] J. R. Dennis and E. B. Hale, Radiat. Eff. **20**, 219 (1976).
[181] D. A. Thompson, Radiat. Eff. **56**, 105 (1981).
[182] J. Narayan, O. S. Oen, D. Fathy, and O. W. Holland, Mater. Lett. **3**, 67 (1985).
[183] M. Avrami, J. Chem. Phys. **9**, 177 (1941).
[184] F. Spaepen and D. Turnbull, in *Laser Annealing of Semiconductors*, edited by J. M. Poate and J. W. Mayer (Academic, New York, 1982).
[185] G. W. Lu, E. Nygren, and M. J. Aziz, J. Appl. Phys. **70**, 5323 (1991).
[186] G. Holmen, J. Linnros, and B. Svensson, Appl. Phys. Lett. **45**, 1116 (1984).
[187] J. Linnros, G. Holmen, and B. Svensson, Phys. Rev. B **32**, 2770 (1985).
[188] F. L. Vook and H. J. Stein, Radiat. Eff. **2**, 23 (1969).
[189] D. J. Chadi and K. J. Chang, Phys. Rev. B **38**, 1523 (1988).
[190] S. Takeda, J. Yamasaki, and Y. Kimura, Physica B **273-274**, 476 (1999).
[191] N. Arai, S. Takeda, and M. Kohyama, Phys. Rev. Lett. **78**, 4265 (1997).
[192] S. Kugler, G. Molnar, G. Peto, E. Zsoldos, L. Rosta, A. Menelle, and R. Bellissent, Phys. Rev. B **40**, 8030 (1989).
[193] W. A. Kamitakahara, H. R. Shank, J. F. McClelland, U. Buchenau, F. Gompf, and L. Pintschovins, Phys. Rev. Lett. **52**, 644 (1984).
[194] M. Tang, L. Colombo, J. Zhu, and T. D. de la Rubia, Phys. Rev. B **55**, 14279 (1997).
[195] F. Cargnoni, C. Gatti, and L. Colombo, Phys. Rev. B **57**, 170 (1998).
[196] S. Goedecker, T. Deutsch, and L. Billard, Phys. Rev. Lett. **88**, 235501 (2002).
[197] D. M. Stock, B. Weber, and K. Gärtner, Phys. Rev. B **61**, 8150 (2000).
[198] B. Weber, D. M. Stock, and K. Gärtner, Mater. Sci. Eng., B **B71**, 213 (2000).
[199] M. Ishimaru, S. Munetoh, T. Motooka, K. Moriguchi, and A. Shintani, Phys. Rev. B **58**, 12583 (1998).
[200] L. A. Marqués, L. Pelaz, J. Hernández, J. Barbolla, and G. H. Gilmer, Phys. Rev. B **64**, 45214 (2001).
[201] J. Tersoff, Phys. Rev. B **38**, 9902 (1988).
[202] L. A. Marqués, L. Pelaz, M. Aboy, and J. Barbolla, Nucl. Instrum. Methods Phys. Res. B **216**, 57 (2004).
[203] M. Ishimaru, S. Munetoh, and T. Motooka, Phys. Rev. B **56**, 15133 (1997).
[204] J. K. Bording and J. Taftø, Phys. Rev. B **62**, 8098 (2000).
[205] K. M. Beardmore and N. Grønbech-Jensen, Phys. Rev. B **60**, 12610 (1999).
[206] M. Koster and H. Urbassek, Phys. Rev. B **62**, 11219 (2000).
[207] K. Nordlund and R. S. Averback, Phys. Rev. B **56**, 2421 (1997).
[208] J. W. Mayer and S. S. Lau, *Electronics Materials Science for Integrated Circuits in Si and GaAs* (MacMillan, New York, 1990).
[209] L. J. Porter, S. Yip, M. Yamaguchi, H. Kaburaki, and M. Tang, J. Appl. Phys. **81**, 96 (1997).
[210] C. Spinella, S. Lombardo, and S. U. Campisano, Appl. Surf. Sci. **43**, 187 (1989).
[211] J. H. Shin and H. A. Atwater, Nucl. Instrum. Methods Phys. Res. B **80/81**, 973 (1993).
[212] L. A. Marqués, L. Pelaz, M. Aboy, L. Enríquez, and J. Barbolla, Phys. Rev. Lett. **91**, 135504 (2003).
[213] L. J. Lewis and R. M. Nieminen, Phys. Rev. B **54**, 1459 (1996).
[214] L. Pelaz, L. A. Marques, M. Aboy, J. Barbolla, and G. H. Gilmer, Appl. Phys. Lett. **82**, 2038 (2003).
[215] K. Nordlund, M. Ghaly, R. S. Averback, M.-J. Caturla, T. D. de la Rubia, and J. Tarus, Phys. Rev. B **57**, 7556 (1998).
[216] M. Giles, J. Electrochem. Soc. **138**, 1160 (1991).
[217] L. Pelaz, G. H. Gilmer, V. C. Venezia, H.-J. Gossmann, M. Jaraiz, and J. Barbolla, Appl. Phys. Lett. **74**, 2017 (1999).
[218] R. G. Elliman, J. M. Gibson, D. C. Jacobson, J. M. Poate, and J. S. Williams, Appl. Phys. Lett. **46**, 478 (1985).
[219] J. M. Poate, D. C. Jacobson, J. S. Williams, R. G. Elliman, and D. O. Boerma, Nucl. Instrum. Methods Phys. Res. B **19–20**, 480 (1987).
[220] D. C. Jacobson, R. G. Elliman, J. M. Gibson, G. L. Olson, J. M. Poate, and J. S. Williams, in *Beam-solid Interactions and Transient Processing*, edited by Michael O. Thompson, S. Thomas Picraux, and James S. Williams, MRS Symposia Proceedings No. 74 (Materials Research Society, Pittsburgh, 1987), p. 327.
[221] A. Polman, D. C. Jacobson, S. Coffa, J. M. Poate, S. Roorda, and W. C. Sinke, Appl. Phys. Lett. **57**, 1230 (1990).
[222] V. C. Venezia *et al.*, Proceedings of IEEE International Electron Devices Meeting 2003.
[223] S. Whelan, V. Privitera, G. Mannino, M. Italia, C. Bongiorno, A. La-Magna, and E. Napolitani, J. Appl. Phys. **90**, 3873 (2001).
[224] B. J. Pawlak *et al.*, J. Vac. Sci. Technol. B **22**, 297 (2004).
[225] A. Mattoni and L. Colombo, Phys. Rev. B **69**, 45204 (2004).

**Downloaded 28 Oct 2008 to 192.84.153.250. Redistribution subject to AIP license or copyright; see http://jap.aip.org/jap/copyright.jsp**